Precambrian Research 231 (2013) 325–342

Contents lists available at SciVerse ScienceDirect

Precambrian Research

journal homepage: www.elsevier.com/locate/precamres

Early Neoproterozoic (~850 Ma) back-arc basin in the Central Jiangnan Orogen (Eastern South China): Geochronological and petrogenetic constraints from meta-basalts

Yuzhi Zhang[a,b], Yuejun Wang[a,*], Hongyan Geng[c], Yanhua Zhang[d], Weiming Fan[a], Hong Zhong[e]

[a] State Key Laboratory of Isotope Geochemistry, Guangzhou Institute of Geochemistry, Chinese Academy of Sciences, Guangzhou 510640, China
[b] Graduate University of Chinese Academy of Sciences, Beijing 100049, China
[c] Department of Earth Sciences, The University of Hong Kong, Pokfulam Road, Hong Kong
[d] CSIRO Earth Sciences and Resource Engineering, Bentley, WA 6102, Australia
[e] State Key Laboratory of Ore Deport Geochemistry, Institute of Geochemistry, Chinese Academy of Sciences, Guiyang 550002, China

ARTICLE INFO

Article history:
Received 6 December 2012
Received in revised form 19 March 2013
Accepted 20 March 2013
Available online 29 March 2013

Keywords:
Early Neoproterozoic time
Zircon U–Pb geochronology
MORB source with arc-like signatures
Back-arc basin
Central Jiangnan Orogen

ABSTRACT

The Neoproterozoic mafic rocks of the Jiangnan Orogen in South China provide a critical geological record for unraveling regional tectonic history and testing different tectonic models. However, the geochronology, geochemistry and petrogenesis of >835 Ma mafic igneous rocks in the Central and Southwestern Jiangnan Orogen have not been well reported so far, in contrast to the extensive study of such rocks in the Eastern Jiangnan Orogen. An integrated study of geochronology and geochemistry has been carried out for the basaltic rocks from NE Hunan and NW Jiangxi Provinces of the Central Jiangnan Orogen. SHRIMP, SIMS and LA-ICP-MS zircon U–Pb dating of three mafic samples yielded zircon U–Pb ages of 860 ± 20 Ma, 838 ± 12 Ma and 847 ± 18 Ma, respectively. This provides evidence for the development of early Neoproterozoic (~850 Ma) mafic lava along the Central Jiangnan Orogen. SiO_2 ranges from 49.43 wt% to 52.07 wt% and MgO from 7.36 wt% to 9.04 wt% with *mg*-number of 68–57. Their chondrite-normalized REE patterns exhibit a left-sloping pattern with more depleted LREEs relative to HREEs. On the N-MORB-normalized multi-element patterns, they are characterized by enriched highly incompatible elements, depleted moderately incompatible elements relative to those in N-MORB, insignificant Nb–Ta depletion and remarkably positive Sr and weakly negative Ti anomalies, resembling those of modern Eastern Lau back-arc basin basalts. In addition, these rocks have positive $\varepsilon_{Nd}(t)$ values of 1.30–9.36 with initial $^{87}Sr/^{86}Sr$ ratios in the range of 0.70796–0.71126. The geochemical characteristics above indicate an origination of the MORB-like source modified by the flux of the slab-derived fluid and input of the recycled sediment-derived melt. This finding, together with other geological observations, suggests that the mafic rocks in the Central Jiangnan Orogen might be formed in a back-arc basin in the eastern SCB. In conjunction with other data, it is inferred that the closure of the back-arc basin along the Central Jiangnan Orogen is contemporaneous with that in the Fuchuan area.

1. Introduction

The united South China Block (SCB) is commonly accepted as the result of the amalgamation of the Yangtze Block to the northwest and Cathaysia Block to the southeast along the Jiangnan Orogen (also named Jiangnan oldland) during the Neoproterozoic period (e.g., Charvet et al., 1996; Zhao and Cawood, 1999, 2012; Li et al., 2002, 2003, 2008a, 2009a; Wang et al., 2006, 2007; Ye et al., 2007; Shu et al., 2011; Xia et al., 2012; Yu et al., 2012). The orogenic belt can be geographically subdivided into the Eastern (NE Jiangxi and north Zhejiang), Central (NW Jiangxi and NE Hunan) and Southwestern (west Hunan and north Guangxi Provinces) Jiangnan Orogen (Fig. 1a). The amalgamation history along the belt has attracted much attention since the SCB has been proposed as the "missing-link" between Australia and Laurentia during the assembly and breakup of the Rodinia (e.g., Li et al., 1995, 2002, 2008b, 2010).

A number of lines of evidence show that, in the Zhangshudun-Shuangxiwu areas in NE Jiangxi and north Zhejiang Provinces of the Eastern Jiangnan Orogen, there occurred an earliest Neoproterozoic (~920–970 Ma) back-arc or intraoceanic arc system (e.g., Li and Li, 2003; Li et al., 2002, 2008a, 2009a; Ye et al., 2007). However, in north Guangxi, west and NE Hunan and NW Jiangxi Provinces of the Central and Southwestern Jiangnan Orogen, the

* Corresponding author at: Guangzhou Institute of Geochemistry, Chinese Academy of Sciences, P.O. Box 1131, Guangzhou 510640, China.
Tel.: +86 20 85290527; fax: +86 20 85290527.
E-mail address: yjwang@gig.ac.cn (Y. Wang).

0301-9268/$ – see front matter © 2013 Elsevier B.V. All rights reserved.
http://dx.doi.org/10.1016/j.precamres.2013.03.016

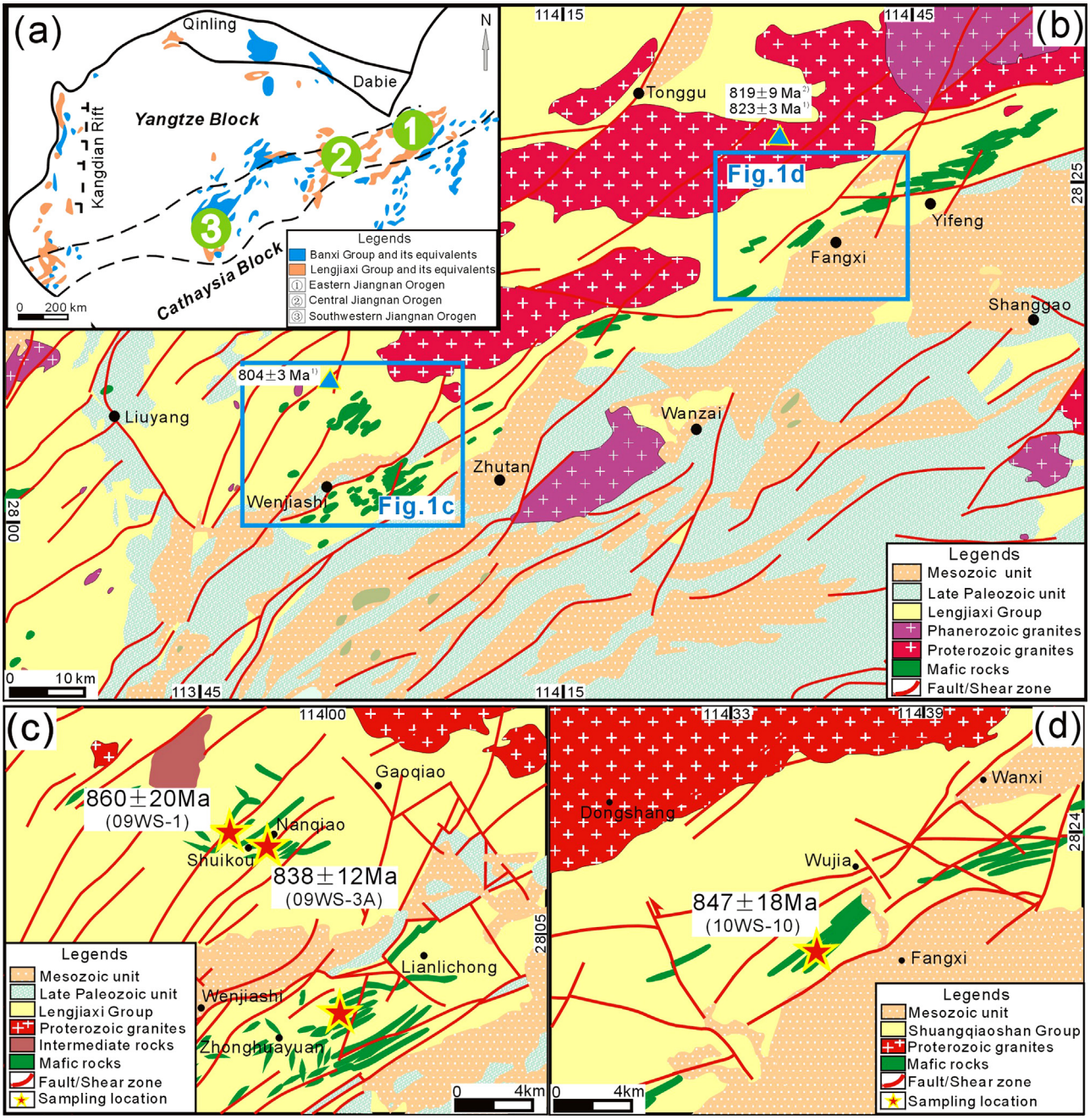

Fig. 1. (a) Simplified geological map of the Yangtze Block showing the Jiangnan Orogen (modified after Zheng et al., 2007; Ma et al., 2002), which is subdivided into the Eastern (1), Central (2) and Southwestern (3) Orogens. (b) Geological map of NE Hunan and NW Jiangxi Provinces of the Central Jiangnan Orogen. (c and d) Simplified geological map of the Wenjiashi and Yifeng area (modified after Hunan BGMR, 1988; Jiangxi BGMR, 1984). Sources for the quoted granitic ages are from Zhang et al. (2011a) and Li et al. (2003).

presence of >835 Ma mafic igneous rock have been poorly reported so far, distinct from the Zhangshudun-Shuangxiwu area of the Eastern Jiangnan Orogen where such rocks are rather extensive (e.g., Zhou et al., 2009; Li et al., 2002, 2008a, 2009a; Ye et al., 2007). In contrast, there are numerous mafic and granitic rocks with the crystallization ages of 835–750 Ma (with majority at 830–800 Ma) along the Central and Southwestern Jiangnan Orogen, which are linked to post-collision, rifting or plume settings (e.g., Wang et al., 2006, 2011a,b, 2012a, 2012b; Zhou et al., 2009; Ma et al., 2009; Zhang et al., 2009, 2011a, 2011b, 2012b; Zhong et al., 2005; Dong et al., 2010, 2011, 2012; Zhao et al., 2011). However, the sandstones in the Lengjiaxi Group and its equivalents (the Sibao Group in Guangxi, Fanjingshan Group in Guizhou and Shuangqiaoshan Group in Jiangxi Provinces) as well as even lower Paleozoic units along the Central and Southwestern Jiangnan Orogen preserved abundant 850–880 Ma detrital zircons but rare ~1.0 Ga grains (e.g., Wang et al., 2007, 2010, 2012c, 2012d, in press; Zhou et al., 2009; Zhao et al., 2011). This led to the major controversy over the convergent history of the Yangtze and Cathaysia Blocks, the timing of final amalgamation (~880 Ma vs. ~820 Ma vs. ~800 Ma) and the geodynamic mechanism (subduction-collision vs. plume vs. plate-rift models) (e.g., Li et al., 1995, 2002, 2008a, 2009a; Ye et al., 2007; Wang et al., 2006, 2008a; Zheng et al., 2007; Zhao et al., 2011; Zhang et al., 2012b; Zhao and Cawood, 2012 and reference therein).

The Neoproterozoic mafic rocks within the Central and Southwestern Jiangnan Orogen are critical to unraveling regional tectonic

history and test different tectonic models. Previous studies focused on the mafic-ultramafic rocks with the formation ages of less than 835 Ma in the Fanjinshan and Sibao Groups in the Southwestern Jiangnan Orogen (e.g., Li et al., 1999, 2003, 2004; Zhou et al., 2004, 2009; Wang et al., 2006, 2008a, 2012b; Zheng et al., 2006, 2008; Zhang et al., 2012b). However, less attention has been paid to the mafic rocks in the Lengjiaxi Group in NE Hunan and the Shuangqiaoshan Group in NW Jiangxi Provinces of the Central Jiangnan Orogen, about which the tectonic regime is still in dispute. Our field investigations show that small amounts of layered or stratoid basaltic rocks occurred in the Lengjiaxi and Shuangqiaoshan Groups along the Central Jiangnan Orogen. In this paper, we present the results of our new geochronological and petrogenetic analyses on these rocks and discuss their implications on the tectonic settings.

2. Geological background and petrology

The Jiangnan Orogen extends geographically from northeastern Jiangxi through southern Jiuling (northwestern Jiangxi) and to eastern Xuefengshan (western Hunan) and then to the Miaoling Mountain (northeastern Guangxi). It is an ENE-trending tectonic belt, with a width of 80–120 km and a strike-length of over 1000 km, along the eastern margin of the Yangtze Block (Fig. 1a, Hunan BGMR, 1988; Jiangxi BGMR, 1984). This belt is considered to be a continental-continental orogen, along which the Yangtze and Cathaysia Blocks amalgamated to form the coherent SCB during the early Neoproterozoic time (e.g., Charvet et al., 1996; Shu et al., 2006, 2011; Wang et al., 2008a; Zhao and Guo, 2012). Li et al. (1999, 2002, 2008b) named it the Sibao (~1.0 Ga) Orogen associated with the assembly of Rodinia, occupying an intra-cratonic keystone position between Australia and Laurentia. Along the belt, the Precambrian sequences comprise the extensively-outcropped Neoproterozoic Lengjiaxi Group, Banxi Group and their equivalents as well as the Sinian units (e.g., Pan, 2001; Hunan BGMR, 1988).

The Lengjiaxi Group and its equivalents (e.g., Shuangqiaoshan Group in NW Jiangxi; Sibao Group in NE Guangxi and Fanjingshan Group in SE Guizhou Provinces) experienced a multiple phase of structural overprinting as marked by tight linear folds and isoclinal overturned folds. They were traditionally considered the folded basement of the Jiangnan orogenic belt, which is characterized by the greenschist-facies metamorphism with the metamorphic temperature and pressure of 300–450 °C and 4–6 kbar, respectively (e.g., Hunan BGMR, 1988). The lithology of the Lengjiaxi Group and its equivalents is dominated by volcanic–sedimentary sequences with tholeiitic mafic lavas at the lower segment and flysch turbidite at the upper segment. The turbidite sequence is more than 25,000 m thick, and consists of metamorphic sandstone, siltstone, tuff, schist, phyllite and slate. Available data show that the bentonite and sandstone of the Lengjiaxi Group and its equivalents yielded a zircon U–Pb eruption age of 822–850 Ma and the youngest detrital zircon U–Pb age-cluster of 850–870 Ma, respectively (Zhao et al., 2011; Zhou et al., 2009; Gao et al., 2008, 2010, 2011). At the top of the Lengjiaxi Group in west Hunan, there is a volcanoclastic unit named the Cangshuipu Group that is composed of the Linjiawan red-polymictic conglomerate and Yinzhuba terrestrial volcanic agglomerate (e.g., Pan et al., 1988; Pan, 2001; Zhang et al., 2011b, 2012b). The part of the volcanic unit is characterized by high-mg andesites formed in a collisional setting and dated at 822–825 Ma. The conglomerate is considered as the indicator of the final assemblage of the Yangtze and Cathaysia Blocks (e.g., Zhang et al., 2012b and reference therein).

The Banxi Group and its equivalents overlie the Lengjiaxi Group with an angular unconformity. They are characterized by well-bedded greywacke, conglomerate, sandstone, limestone, siltstones, schist, shale and tuff, and are commonly considered a sedimentary package deposited in a long-term but failed rift setting (e.g., Hunan BGMR, 1988; Chen and Jahn, 1998; Wang et al., 2003a, 2006; Wang and Li, 2003). The Banxi Group and its equivalents underwent a lower greenschist-facies metamorphism and preserve abundant upright and open folds, distinct from those of the Leangjiaxi Group and its equivalents.

Precambrian igneous rocks along the Jiangnan Orogen contain a small amount of mafic-ultramafic plutons and tholeiitic basalts in the Lengjiaxi Group and voluminous peraluminous granites (e.g., Wang and Li, 2003). The granitic batholiths are dominated by peraluminous K-feldspar granites and two-mica granites with porphyritic to porphyroid textures, along with the mineral assemblages of quartz, K-feldspar, plagioclase and minor biotite, muscovite as well as accessory minerals. Available geochronological data show that the Precambrian granites have the zircon U–Pb crystallization ages of 745–825 Ma with two age-peaks of ~770 and ~820 Ma (e.g., Xu and Zhou, 1992; Tang et al., 1997; Liu, 1997; Li, 1999; Li et al., 1999, 2002, 2003; Wu et al., 2006; Zheng et al., 2007, 2008 and references therein). The mafic- ultramafic plutons are mainly exposed in the Wanzai-Nanchang (NW Jiangxi), Huaihua -Yiyang-Liuyang (west Hunan) and Longsheng (south Guangxi) areas. They are preserved as dykes and layered sills mainly in the Lengjiaxi Group, with only several dykes observed in the Banxi Group (e.g., Hunan BGMR, 1988; Wang et al., 2004, 2007). The Precambrian basaltic rocks in the Jiangnan Orogen mainly occurred at the lower segment of the Lengjiaxi Group and its equivalents. They usually show pillow structure with the primary mineral association of plagioclases, pyroxenes and fewer magnetites, as observed in the Fanjingshan (Guizhou) and Yiyang (Hunan) basaltic pillow lavas.

The Central Jiangnan Orogen in northeast Hunan and west Jiangxi has a strike-length of over 120 km and is an area bridging the Eastern Jiangnan and SW Jiangnan Orogen (Fig. 1b). In this orogenic belt, there are abundant mafic rocks in the Lengjiaxi and Shuangqiaoshan Groups (NE Hunan and western Jiangxi), constituting an ENE-trending zone of mafic rocks (Figs. 1b–d). To the northwest side of the zone, is marked by the 823–804 Ma Jiuling granitic batholith with an exposed area of ~2500 km^2 (Li et al., 2003; Zhang et al., 2011a). To the southeast side the outcropped rocks are characterized by the upper Paleozoic siliciclastic strata (Fig. 1b). Previous studies usually mapped the mafic rocks as the parallel gabbro and diabase dykes, with widths of about 2–7 m for individual dykes, in spite that some geological, geochemical and geochronological data for the mafic rocks have been reported. Our field investigation shows that the majority of the mafic rocks are basaltic lava involving pillow basalt, spilite, dolerite, coarse-grained basaltic andesite and tuff, which are interlayered and stratoid in the greenschist-facies sedimentary sequences of the Lengjiaxi and Shuangqiaoshan Groups (Fig. 2a and b, Jiangxi BGMR, 1984; Hunan BGMR, 1988; Wang et al., 2008a; Zhou et al., 2009). These mafic rocks are grayish green to dark grayish green and show a blastodiabastic texture. They were often folded together with the inclosing sedimentary strata and underwent greenschist-facies metamorphism (e.g., Jiangxi BGMR, 1984; Hunan BGMR, 1988). The mineral assemblages of the meta-basalts include 25–40% phenocrysts 53–62% matrix, with phenocrysts being 15–20% clinopyroxene and 10–20% plagioclase and matrix containing fine-grained to aphanitic groundmass of plagioclase, clinopyroxene and minor apatite, ilmenite, sphene and titanite (Fig. 2c and d). Plagioclase was usually altered. The basaltic samples in this study are basalt and dolerite interlayered in the slate, sandstone and phyllite in the lower part of the Lengjiaxi and Shuangqiaoshan Groups (Fig. 2a and b). They were collected from Shuikou and Nanqiao villages in Wenjiashi (Fig. 1c, NE Hunan), Zhonghuayuan at the border of NE Hunan

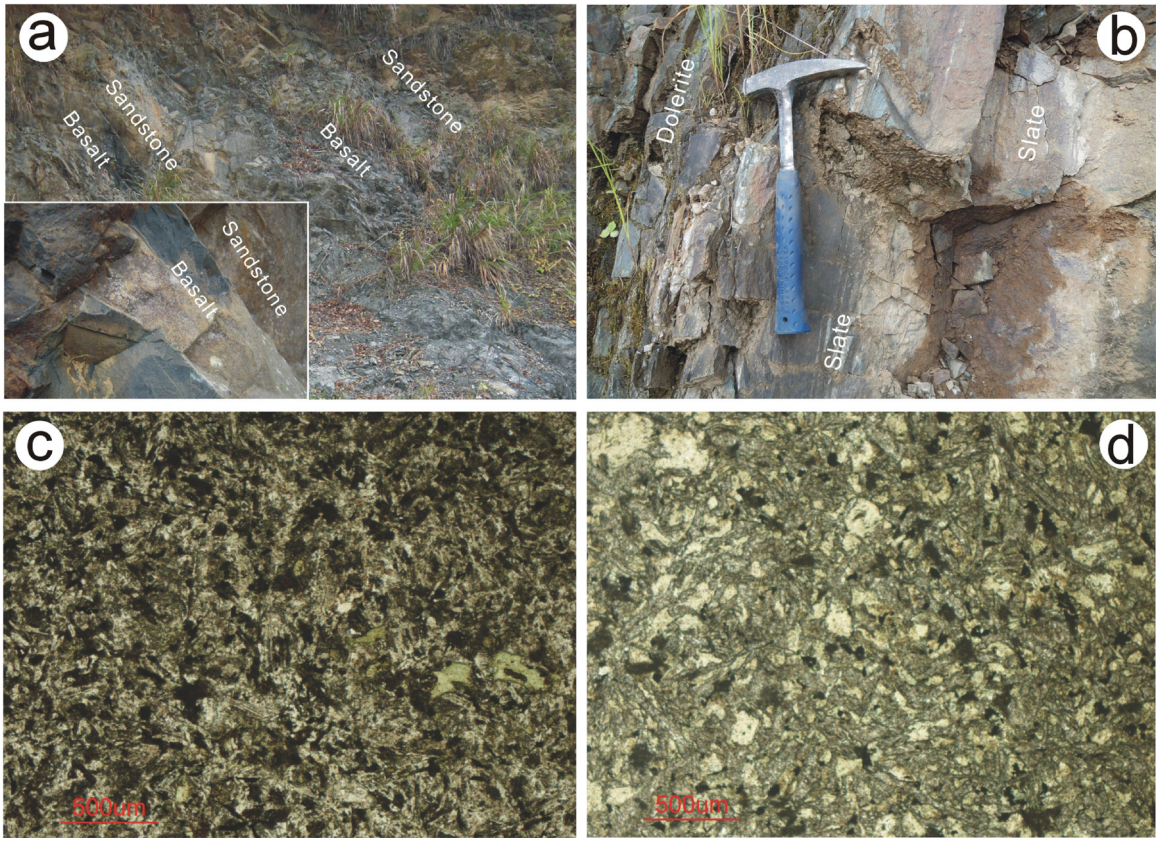

Fig. 2. Field and microscopic photographs for Shuikou basalt (a and c) and Fangxi dolerite (b and d) interlayered in the Lengjiaxi and Shuangqiaoshan sequences, repectively.

with west Jiangxi and Fangxi in Yifeng (Fig. 1c and d, western Jiangxi).

3. Analytical methods

The first step of sample preparation is to remove weathered rims. The samples were then pulverized to 200-mesh using an agate mill for elemental and isotopic analyses. The contents of major oxides were measured by a wavelength X-ray fluorescence spectrometry at the Guangzhou Institute of Geochemistry (GIG), Chinese Academy of Sciences (CAS). Details of procedures were described by Li et al. (2005). Trace element abundances were analyzed using inductively coupled plasma mass spectrometer (ICP-MS) at GIG, CAS. Detailed sample preparation and analytical procedure followed Wei et al. (2002). Samples powders for Sr and Nd isotopic analyses were spiked with mixed isotope tracers, dissolved in Teflon capsules with $HF + HNO_3$ acids, separated by the conventional cation-exchange technique and run on single W and Ta–Re double filaments. Sr–Nd Isotope ratios were measured on the VG-354 mass-spectrometer at GIG, CAS. Sample preparation and chemical separation followed Liang et al. (2003). The total procedure blanks were in the range of 200–500 pg for Sr and $\leq$50 pg for Nd. The mass fractionation corrections for Sr and Nd isotopic ratios are based on $^{86}Sr/^{88}Sr = 0.1194$ and $^{146}Nd/^{144}Nd = 0.7219$, respectively. The measured $^{87}Sr/^{86}Sr$ ratio of the (NIST) SRM 987 standard is 0.710265 ± 12 (2σ) and the $^{143}Nd/^{144}Nd$ ratio of the La Jolla standard is 0.511862 ± 10 (2σ).

Zircon grains were separated using standard density and magnetic separation techniques, and then handpicked under a binocular microscope. The grains were mounted in epoxy, polished and coated with gold. The reflected and transmitted light and cathodoluminescene (CL) imaging was carried out using a JXA-8100 electron probe microanalyzer at GIG, CAS to investigate the internal texture of zircons. In this study, SHRIMP, SIMS and LA-MC-ICP-MS zircon U–Pb dating methods were adopted. U, Th and Pb isotopic measurements for 09WS-1, 09WS-3A and 10WS-10 were undertaken using the Sensitive High-Resolution Ion Microprobe (SHRIMP-II) at the Beijing SHRIMP Center (Chinese Academy of Geological Sciences), Cameca IMS 1280 large-radius SIMS at the Institute of Geology and Geophysics (CAS) and Nu instruments MC-ICP-MS, attached to the Resonetics RESOlution M-50-HR Excimer Laser Ablation System at the Department of Earth Sciences, the University of Hong Kong, respectively. The instrumental setting and detailed analytical procedures for three dating techniques were described in Song et al. (2002), Li et al. (2009b), and Xia et al. (2011), respectively. Common Pb correction was made using the observed ^{204}Pb peak (Compston et al., 1984). The errors for individual U–Pb analyses are presented with 2σ error in data tables and in concordia diagrams and out using the SQUID) 1.03 and Isoplot/Ex 2.49 programs of Ludwig (2001).

4. Zircon U–Pb geochronology

Two basaltic samples from Shuikou (09WS-1) and Nanqiao (09WS-3A) and a dolerite sample from Fangxi (10WS-10) are selected for SHRIMP, SIMS and LA-ICP-MS zircon U–Pb dating, respectively. The corresponding dating results are presented in Tables 1 and 2. The sampling location, outcrop and microscope photos for these samples are shown in Figs. 1 and 2.

4.1. Shuikou basalt (09WS-1)

Zircon grains separated from this sample are euhedral, colorless, either prismatic or ellipsoidal with weak oscillatory zoning (inset in

Table 1
SHRIMP and SIMS zircon U–Pb dating results for the Shuikou and Nanqiao basaltic rocks in the Central Jiangnan Orogen.

Spot#	[U] ppm	[Th] ppm	Th/U ratio	[Pb] ppm	$^{207}Pb/^{206}U$	±%	$^{207}Pb/^{235}U$	±%	$^{206}Pb/^{238}U$	±%	$^{206}Pb/^{238}U$	±1σ	$^{207}Pb/^{235}U$	±1σ	$^{207}Pb/^{206}Pb$	±1σ	Disc
09WS-1 (Shuikou, Wenjiashi), SHRIMP zircon U–Pb dating result																	
C1.1	407	1977	5.02	50.4	0.0656	2.3	1.298	4.2	0.1435	3.6	864	29	845	49	795795	48 48	109
C2.1	541	1631	3.12	64.4	0.0676	1.7	1.290	3.9	0.1383	3.6	835	28	841	45	857857	35 35	97
C3.1	311	887	2.95	38.6	0.0615	3.4	1.216	5.0	0.1434	3.6	864	29	808	56	657657	73 73	132
C4.1	568	1635	2.97	72.2	0.0638	1.6	1.295	3.9	0.1472	3.5	885	29	844	45	736736	35 35	120
C5.1	172	282	1.70	20.5	0.0652	6.3	1.235	7.3	0.1375	3.7	830	29	817	84	779779	130 130	107
C6.1	668	1645	2.54	84.5	0.0653	1.9	1.320	4.0	0.1467	3.6	882	29	855	47	783783	40 40	113
C7.1	289	1171	4.19	35.7	0.0627	3.6	1.234	5.1	0.1427	3.6	860	29	816	58	699699	77 77	123
09WS-3A (Nanqiao, Wenjiashi), SIMS zircon U–Pb dating result																	
09WS-3A-1	15	14	0.90	7	0.1087	3.39	4.6012	4.44	0.3175	1.53	1777	24	1749	38	1716	75	104
09WS-3A-2	14	12	0.87	6	0.1062	2.87	4.2220	4.12	0.3032	1.58	1707	24	1678	34	1642	69	104
09WS-3A-3	65	48	0.74	26	0.1099	1.32	4.5901	2.12	0.3078	1.53	1730	23	1747	18	1768	26	98
09WS-3A-4	26	31	1.19	11	0.1065	2.10	4.4245	2.97	0.3112	1.52	1747	23	1717	25	1681	46	104
09WS-3A-5	7	4	0.60	3	0.1076	4.73	4.2864	5.93	0.3001	1.81	1692	27	1691	50	1689	101	100
09WS-3A-6	10	7	0.77	4	0.1097	3.50	4.2114	5.05	0.2951	1.54	1667	23	1676	42	1688	86	99
09WS-3A-7	10	5	0.54	4	0.1094	3.40	4.2532	5.13	0.3021	1.56	1702	23	1684	43	1663	88	102
09WS-3A-8	19	19	0.98	8	0.1072	2.58	4.2269	3.19	0.2901	1.53	1642	22	1679	27	1726	51	95
09WS-3A-9	6	4	0.62	2	0.1123	4.41	4.5370	5.72	0.3053	1.61	1717	24	1738	49	1763	97	97
09WS-3A-10	19	20	1.06	8	0.1069	2.56	4.5229	3.19	0.3115	1.51	1748	23	1735	27	1720	51	102
09WS-3A-11	22	14	0.67	9	0.1027	2.40	4.3526	3.14	0.3137	1.54	1759	24	1703	26	1636	50	108
09WS-3A-12	30	35	1.16	13	0.1054	2.08	4.2279	3.02	0.3019	1.52	1701	23	1679	25	1653	47	103
09WS-3A-13	15	14	0.92	6	0.1064	3.88	4.6452	4.22	0.3168	1.65	1774	26	1757	36	1738	70	102
09WS-3A-14	10	7	0.69	4	0.1140	3.42	4.9029	3.87	0.3119	1.82	1750	28	1803	33	1864	60	94
09WS-3A-15	14	11	0.80	6	0.1096	3.01	4.6858	3.37	0.3100	1.51	1741	23	1765	29	1793	54	97
09WS-3A-16	31	21	0.68	12	0.1059	2.20	4.3452	2.88	0.3020	1.59	1701	24	1702	24	1703	44	100
09WS-3A-17	88	82	0.93	37	0.1081	1.20	4.5971	1.92	0.3083	1.50	1733	23	1749	16	1768	22	98
09WS-3A-18	20	22	1.13	8	0.1127	2.51	4.5716	3.24	0.3007	1.51	1695	23	1744	27	1804	51	94
09WS-3A-19	38	55	1.48	17	0.1067	1.84	4.3973	2.56	0.3038	1.51	1710	23	1712	21	1714	38	100
09WS-3A-20	103	144	1.39	21	0.0658	2.09	1.2607	2.57	0.1389	1.50	838	12	828	15	801	43	105
09WS-3A-21	13	9	0.71	5	0.1104	3.10	4.7258	3.45	0.3106	1.51	1744	23	1772	29	1805	55	97
09WS-3A-22	27	10	0.37	16	0.1700	1.46	10.6444	2.30	0.4682	1.52	2476	31	2493	22	2506	29	99
09WS-3A-23	161	121	0.75	62	0.1036	0.93	4.1554	1.78	0.2913	1.51	1648	22	1665	15	1687	17	98
09WS-3A-24	32	42	1.31	15	0.1096	1.95	4.5750	2.87	0.3142	1.52	1761	24	1745	24	1725	44	102
09WS-3A-25	249	224	0.90	164	0.1653	0.52	10.7299	1.59	0.4725	1.50	2494	31	2500	15	2505	9	100
09WS-3A-26	168	46	0.28	95	0.1690	0.87	10.6491	1.77	0.4605	1.52	2442	31	2493	17	2535	15	96
09WS-3A-27	64	63	0.98	28	0.1066	1.43	4.5644	2.21	0.3138	1.60	1759	25	1743	19	1723	28	102
09WS-3A-28	189	86	0.45	115	0.1712	0.79	11.2029	1.70	0.4754	1.50	2507	31	2540	16	2567	13	98

Table 2
LA-MC-ICP-MS zircon U–Pb dating results for the Fangxi dolerite in the Central Jiangnan Orogen.

Spot#	Th/U ratio	$^{207}Pb/^{206}U$	±1σ	$^{207}Pb/^{235}U$	±1σ	$^{206}Pb/^{238}U$	±1σ	$^{206}Pb/^{238}U$	±1σ	$^{207}Pb/^{235}U$	±1σ	$^{207}Pb/^{206}Pb$	±1σ	Disc
10WS-10 (Fangxi, Yifeng), LA-MC-ICP-MS zircon U–Pb dating result														
10WS-10-01	0.44	0.0675	0.0014	1.2515	0.0291	0.1344	0.0031	813	18	824	13	854	43	95
10WS-10-02	0.74	0.0686	0.0014	1.2071	0.0268	0.1276	0.0027	774	16	804	12	887	43	87
10WS-10-03	0.82	0.0705	0.0017	1.0320	0.0268	0.1061	0.0024	650	14	720	13	944	48	69
10WS-10-04	1.48	0.1654	0.0033	10.7815	0.2476	0.4728	0.0109	2496	48	2504	21	2522	35	99
10WS-10-05	0.38	0.1096	0.0022	4.5895	0.1135	0.3036	0.0075	1709	37	1747	21	1794	31	95
10WS-10-06	0.59	0.0681	0.0014	1.1993	0.0279	0.1277	0.0029	775	17	800	13	872	43	89
10WS-10-07	0.60	0.0699	0.0016	1.2191	0.0313	0.1265	0.0029	768	17	809	14	924	45	83
10WS-10-08	0.57	0.0702	0.0016	1.1514	0.0273	0.1189	0.0026	724	15	778	13	1000	51	72
10WS-10-09	0.51	0.1631	0.0035	10.1789	0.3055	0.4508	0.0117	2399	52	2451	28	2489	36	96
10WS-10-10	0.60	0.0703	0.0018	1.2173	0.0317	0.1256	0.0028	763	16	809	15	937	52	81
10WS-10-11	0.67	0.0675	0.0014	1.3269	0.0321	0.1426	0.0035	859	20	858	14	854	43	101
10WS-10-12	0.87	0.0687	0.0014	1.2269	0.0298	0.1295	0.0032	785	18	813	14	900	38	87
10WS-10-13	0.58	0.0712	0.0016	1.2250	0.0320	0.1248	0.0028	758	16	812	15	963	47	79
10WS-10-14	1.25	0.0691	0.0015	1.1329	0.0262	0.1189	0.0027	724	15	769	12	902	43	80
10WS-10-15	0.64	0.0682	0.0014	1.3201	0.0316	0.1404	0.0033	847	19	855	14	874	43	97
10WS-10-16	1.08	0.0660	0.0013	1.1353	0.0249	0.1248	0.0027	758	15	770	12	806	47	94
10WS-10-17	0.67	0.0666	0.0014	1.1766	0.0260	0.1282	0.0028	778	16	790	12	833	44	93
10WS-10-18	0.46	0.0671	0.0014	1.1723	0.0253	0.1267	0.0027	769	15	788	12	843	43	91
10WS-10-19	1.08	0.0671	0.0014	1.2315	0.0286	0.1332	0.0031	806	18	815	13	840	43	96
10WS-10-20	0.26	0.0675	0.0014	1.2759	0.0304	0.1370	0.0032	828	18	835	14	854	43	97
10WS-10-21	0.56	0.0670	0.0014	1.2906	0.0313	0.1398	0.0034	843	19	842	14	835	43	101
10WS-10-22	0.84	0.1663	0.0034	10.8284	0.2519	0.4720	0.0110	2492	48	2509	22	2521	34	99
10WS-10-23	0.64	0.0685	0.0014	1.1966	0.0279	0.1267	0.0029	769	17	799	13	883	43	87
10WS-10-24	0.47	0.1110	0.0022	4.9238	0.1182	0.3215	0.0077	1797	38	1806	20	1817	32	99
10WS-10-25	0.53	0.0675	0.00	1.1368	0.03	0.1220	0.00	742	16	771	12	854	43	87

Fig. 3a.). The SHRIMP zircon U–Pb analyses of seven zircons give U and Th contents ranging from 172 to 668 ppm and 282 to 1977 ppm, respectively, with Th/U ratios of 1.7–5.0. The seven spots form a coherent group and yielded a weighted mean $^{206}Pb/^{238}U$ age of 860 ± 20 Ma with MSWD = 2.1 (Fig. 3a).

4.2. Nanqiao basalt (09WS-3A)

09WS-3A-20 with weak oscillatory zoning (inset in Fig. 3b) gives Th and U content of 144 and 103 ppm with Th/U ratio of 1.39 and yields an apparent $^{206}Pb/^{238}U$ age of 838 ± 12 Ma, representing the crystallization age of the basalt. The majority of the remaining 27 zircons show a texture of inherited cores surrounded by heterogeneous rims or oscillatory zoning (inset in Fig. 3b). Their analyses plot on the concordant line forming two age-clusters (Fig. 3b). One is constituted by four spots with Th/U ratios of 0.28–0.90 and defines a weighted mean $^{207}Pb/^{206}Pb$ age of 2525 ± 47 Ma (MSWD = 5.2). The other is clustered by 23 analyses, which gives the Th/U ratios of 0.54–1.48 and a weighted mean $^{207}Pb/^{206}Pb$ age of 1725 ± 21 Ma (MSWD = 1.5). The two older ages of 2525 ± 47 Ma and 1725 ± 21 Ma can be interpreted as the ages of the xenocrysts.

4.3. Fangxi dolerite (10WS-10)

Twenty-five spots are analyzed and give a wide range of Th/U ratios from 0.38 to 1.48. Three zircons (10WS-10-0910, -04 and -22) yield the Neoarchean $^{207}Pb/^{206}Pb$ ages of 2489 ± 36 Ma, 2522 ± 35 Ma and 2521 ± 34 Ma, respectively, representative of the ages of the xenolithic grains (Fig. 3c). Two zircons (10WS-10-05 and -24) give the Mesoproterozoic $^{207}Pb/^{206}Pb$ ages of 1794 ± 31 Ma and 1817 ± 32 Ma, respectively. The remaining 20 grains show weak oscillatory zoning (inset in Fig. 3c) and yield the younger apparent $^{206}Pb/^{238}U$ ages of less than 900 Ma. These analytical results form a well-defined regression line with the upper intercept age of 847 ± 18 Ma (Fig. 3c), which is considered to be the crystallization age of the Fangxi dolerite.

5. Geochemical results

The elemental and Sr-Nd isotopic results of nineteen representative samples are listed in Table 3. These samples show narrow variation of major oxides with SiO_2 ranging from 49.43 wt% to 52.07 wt% (volatile-free) and MgO from 7.36 wt% to 9.04 wt% with mg-number of 68–57. They have 9.65–13.64 wt% of Fe_2O_3, 13.94–15.55 wt% of Al_2O_3, 0.63–0.94 wt% of TiO_2, and K_2O/Na_2O ratios of 0.05–0.95. In the plots of SiO_2 vs $Na_2O + K_2O$ (Fig. 4a, Maitre et al., 1989) and Zr/TiO_2 Nb/Y vs Zr/TiO_2 (Fig. 4b, Winchester and Floyd, 1977), they fall into the fields of subalkaline basalt and basaltic andesite. A tholeiitic basalt trend is shown in the AFM diagram of Irvine and Baragar (1971) (Fig. 4c). These samples have Cr and Ni contents of 94–336 ppm and 61–126 ppm, respectively. Fe_2O_3, P_2O_5, TiO_2 and V correlates negatively but Al_2O_3 and Cr positively with MgO (Fig. 5a–f).

The chondrite-normalized rare earth element (REE) patterns are shown in Fig. 6a. These samples exhibit a subparallel and generally left-sloping pattern with more depleted LREEs relative to HREEs and insignificant Eu anomalies ($Eu/Eu^* = 0.87–1.3017$). The (La/Sm)cn ratios range form 0.46 to 0.74, (La/Yb)cn from 0.27 to 0.62 and (Gd/Yb)cn from 0.68 to 0.94 (cn herein refers to chondrite-normalized value). They are characterized by the enrichment of highly incompatible elements (from Rb to Th) but depletion of the moderately incompatible elements (from Nb to Ti with exception of Sr) relative to those of N-MORB (Fig. 6b). Their $(Nb/La)_N$ ratios range from 0.58 to 1.20 with an average value of 0.95, near the average N-MORB value. On the N-MORB-normalized diagram (Fig. 6b), our samples exhibit insignificant Nb–Ta depletion and remarkably positive Sr ($Sr/Sr^* = 1.22–5.09$) and weakly negative Ti anomalies ($Ti/Ti^* = 0.60–0.85$; e.g., Sun and McDonough, 1989). Such signatures are distinct from those of arc volcanics and oceanic island basalt. On the contrary, the patterns are similar to those of modern Eastern Lau back-arc basin basalts (e.g., Tian et al., 2008). This similarity is further supported by the left-sloping patterns for the moderately incompatible elements from Zr to Lu in Fig. 6b.

Seven representative samples were selected for Sr–Nd isotopic measurement and the analyzed results are presented in Table 3

Table 3
Elemental and Sr–Nd isotopic analyses for the ~850 Ma Neoproterozoic mafic rocks in the Central Jiangnan Orogen.

	09WS-1	09WS-2	09WS-3A	09WS-3B	09WS-3D	09WS-3E	01WS-3	01WS-4	01WS-5	01WS-8	WS-8A	WS-8D	WS-8E	WS-8F	10WS-1	10WS-4	10WS-6	10WS-8	10WS-10
SiO_2	49.40	47.49	49.81	48.83	49.41	48.92	49.92	49.84	50.07	49.00	50.82	50.18	50.75	50.87	49.44	49.72	49.82	49.25	49.18
Al_2O_3	13.96	14.02	13.57	13.61	13.48	14.86	13.73	13.67	13.70	14.30	14.87	15.10	15.20	15.01	14.21	13.90	14.03	14.25	14.10
CaO	10.77	11.83	9.69	13.28	11.13	7.92	10.70	10.88	10.18	12.01	10.93	10.29	9.71	11.04	11.45	11.31	11.40	10.94	11.99
FeOt	12.36	11.84	12.92	11.18	11.55	13.26	12.33	12.37	12.51	10.71	9.42	9.77	9.68	9.45	10.65	11.23	11.24	11.44	7.78
MgO	7.16	8.20	7.89	8.36	7.99	8.62	7.18	7.22	7.36	8.01	8.49	8.81	8.51	8.55	8.11	7.79	7.78	8.19	11.65
MnO	0.19	0.21	0.20	0.19	0.22	0.22	0.20	0.20	0.20	0.19	0.21	0.19	0.23	0.21	0.19	0.19	0.19	0.19	1.51
K_2O	0.85	0.47	0.48	0.08	0.55	0.59	0.80	0.64	0.93	1.05	0.44	0.70	0.53	0.30	1.25	1.14	1.17	0.23	0.24
Na_2O	1.60	1.34	1.44	1.43	1.52	2.09	1.81	1.89	1.85	1.31	1.70	1.69	2.38	1.66	1.32	1.46	1.42	2.23	0.22
P_2O_5	0.07	0.04	0.07	0.04	0.05	0.05	0.09	0.07	0.09	0.05	0.05	0.04	0.05	0.05	0.05	0.06	0.06	0.05	0.81
TiO_2	0.92	0.65	0.79	0.62	0.69	0.72	0.89	0.90	0.90	0.65	0.68	0.69	0.70	0.68	0.65	0.74	0.71	0.63	0.07
LOI	2.08	3.34	3.02	1.99	2.90	2.12	3.20	3.15	3.13	3.37	1.96	2.13	1.82	1.76	3.36	3.12	2.90	3.35	2.07
Total	99.36	99.43	99.89	99.61	99.49	99.35	99.83	99.83	99.84	99.82	99.56	99.58	99.57	99.57	99.83	99.75	99.81	99.81	99.61
mg#	57	62	59	64	62	60	58	58	58	64	68	68	67	68	64	62	62	63	60
Sc	51.45	50.03	52.35		53.42		46.40	46.57	46.46	48.72	44.70	43.70	45.80	43.10	46.92	42.86	44.07	44.03	46.60
V	305.1	278.2	311.2		274.8		358.9	337.6	333.2	286.1	244.0	237.0	246.0	244.0	278.9	278.5	281.0	316.4	306.0
Cr	94.5	105.0	123.1		176.1		139.7	102.8	200.5	122.1	320.0	336.0	314.0	304.0	152.9	198.4	144.6	128.0	98.4
Co	42.07	58.26	31.82		41.74		39.66	48.74	47.20	47.05	40.40	38.60	35.70	38.20	48.79	47.15	44.77	44.74	40.90
Ni	60.73	83.50	70.42		70.14		78.16	66.98	114.74	80.00	100.00	97.60	107.00	96.30	98.36	125.71	87.08	85.34	70.60
Rb	45.91	24.56	24.73		32.74		53.18	37.99	60.29	69.99	22.50	32.30	35.70	14.10	86.95	70.06	72.22	11.79	15.90
Sr	95.35	107.80	88.86		66.83		112.61	111.75	95.52	95.78	303.00	164.00	270.00	291.00	90.39	110.23	114.21	138.72	77.50
Y	30.33	24.11	31.35		24.82		33.08	32.87	32.15	26.19	27.80	26.40	27.20	26.50	24.50	25.96	36.22	24.82	29.70
Zr	59.61	40.75	50.68		42.72		44.60	43.55	44.03	30.74	41.80	42.00	39.30	40.10	29.89	31.09	33.64	25.13	39.70
Nb	1.51	1.06	1.50		0.88		1.94	1.90	1.98	1.28	1.34	1.33	1.27	1.26	1.29	1.22	1.19	1.26	1.38
Ba	63.4	40.0	41.2		52.0		74.5	57.4	77.0	73.6	145.0	128.0	101.0	93.2	83.3	74.2	73.5	29.5	26.1
La	2.15	1.12	1.62		1.11		1.83	1.90	1.77	1.30	1.69	2.46	1.67	1.70	1.35	1.31	1.27	1.15	4.01
Ce	5.99	3.29	4.95		3.26		5.13	5.52	5.09	3.72	5.04	6.98	5.25	5.06	3.95	3.81	3.75	3.13	4.31
Pr	0.98	0.56	0.87		0.58		0.87	0.89	0.85	0.66	0.90	1.13	0.84	0.85	0.66	0.67	0.63	0.56	1.21
Nd	5.52	3.24	5.00		3.35		4.98	4.89	4.77	3.67	4.95	6.54	4.89	4.70	3.69	3.62	3.57	3.10	5.33
Sm	2.15	1.50	2.15		1.55		2.15	2.07	2.21	1.60	1.99	2.26	1.93	1.78	1.60	1.72	1.62	1.47	2.12
Eu	0.81	0.63	1.02		0.60		0.79	0.82	0.84	0.67	0.76	1.01	1.01	0.76	0.60	0.72	0.67	0.57	0.93
Gd	3.51	2.61	3.62		2.76		3.47	3.42	3.49	2.68	3.25	3.23	2.90	3.15	2.43	2.72	2.63	2.49	3.36
Tb	0.75	0.59	0.81		0.62		0.77	0.78	0.79	0.64	0.61	0.65	0.58	0.61	0.58	0.60	0.60	0.58	0.70
Dy	5.25	4.16	5.50		4.37		5.30	5.00	5.41	4.17	4.24	4.47	4.06	4.06	3.91	4.25	4.09	3.94	5.18
Ho	1.19	0.94	1.25		0.98		1.27	1.22	1.27	0.98	1.05	1.03	1.06	1.02	0.94	1.02	1.03	0.96	1.24
Er	3.45	2.75	3.67		2.96		3.65	3.59	3.60	2.78	3.10	3.06	3.03	2.89	2.87	2.88	2.96	2.93	3.45
Tm	0.52	0.43	0.57		0.45		0.54	0.56	0.56	0.42	0.46	0.43	0.45	0.44	0.40	0.39	0.43	0.43	0.49
Yb	3.57	2.88	3.69		2.95		3.60	3.71	3.69	2.99	2.98	2.84	2.86	2.77	2.82	2.97	3.17	2.97	3.28
Lu	0.54	0.44	0.57		0.46		0.60	0.61	0.60	0.48	0.48	0.43	0.45	0.42	0.48	0.50	0.49	0.47	0.49
Hf	1.75	1.27	1.63		1.30		1.46	1.43	1.51	1.10	1.19	1.17	1.25	1.15	1.06	1.09	1.10	0.89	1.21
Ta	0.13	0.08	0.12		0.07		0.13	0.13	0.14	0.09	0.12	0.10	0.10	0.10	0.10	0.09	0.10	0.08	0.11
Pb	5.54	3.34	2.00		2.75		6.50	5.22	8.84	6.59	11.27	8.27	8.07	10.64	6.03	9.07	7.32	6.38	4.54
Th	0.32	0.11	0.14		0.14		0.21	0.29	0.16	0.12	0.32	0.27	0.18	0.27	0.24	0.11	0.13	0.14	0.14
U	0.07	0.03	0.04		0.04		0.05	0.07	0.04	0.03	0.09	0.07	0.05	0.07	0.04	0.07	0.03	0.04	0.07
$^{87}Rb/^{86}Sr$							1.3693	0.9857			0.2153	0.5710		0.1405			1.8334	0.2464	
$^{147}Sm/^{144}Nd$							0.2611	0.2559			0.2431	0.2122		0.2291			0.2754	0.2877	
$^{87}Sr/^{86}Sr$							0.727048	0.722308			0.713682	0.714894		0.712960			0.733435	0.712914	
2σ							15	14			11	12		12			18	16	
$^{143}Nd/^{144}Nd$							0.513417	0.513373			0.513137	0.512791		0.513113			0.513487	0.513624	
2σ							8	9			10	8		10			9	11	
$^{87}Sr/^{86}Sr(i)$							0.710420	0.710338			0.711068	0.707960		0.711255			0.711172	0.709922	
$\varepsilon_{Nd}(t)$							8.21	7.91			4.70	1.30		5.76			8.01	9.36	

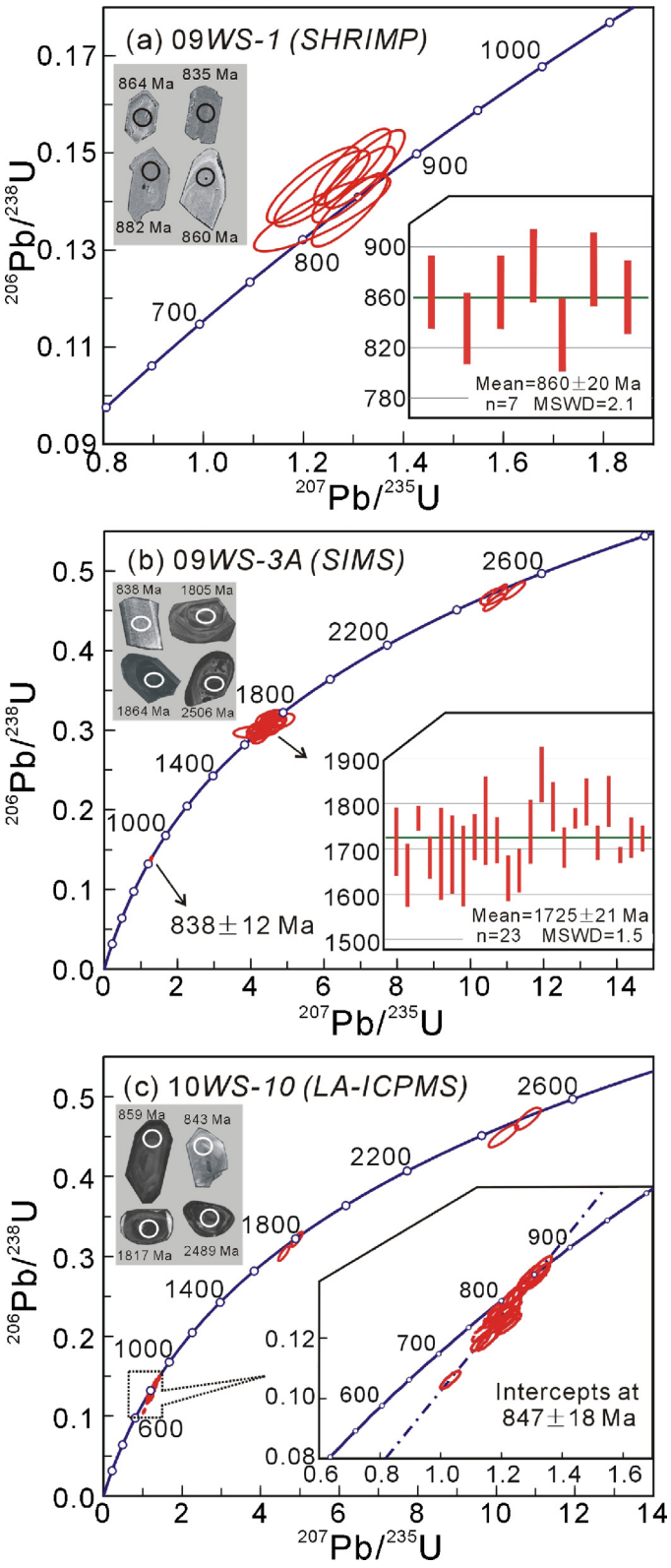

Fig. 3. (a–c) Concordia diagrams of zircon U–Pb data for the Shuikou (09WS-1), Nanqiao (09WS-3A) and Fangxi mafic rocks (10WS-10), respectively along the Central Jiangnan Orogen. Insets in a–c note the representative cathodoluminescence images for zircons.

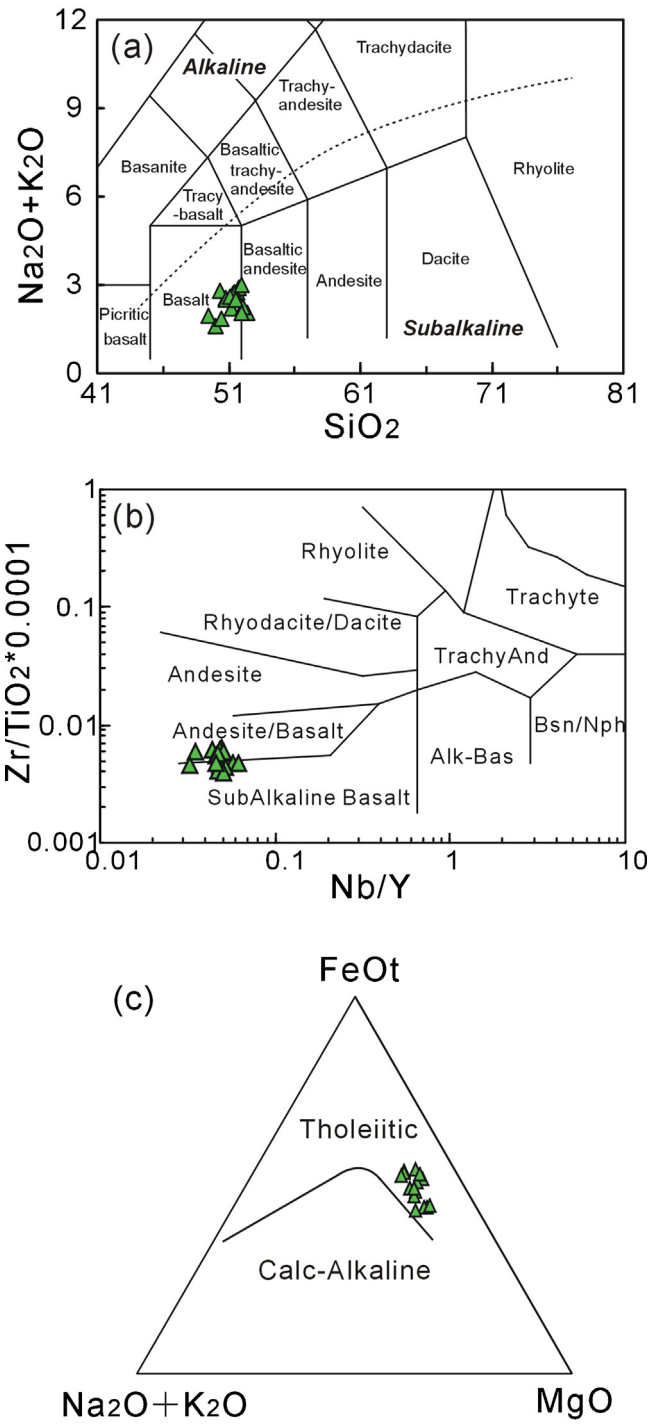

Fig. 4. Rock classification diagrams of (a) TAS diagram (after Maitre et al., 1989), (b) Zr/TiO_2–Nb/Y diagram (after Winchester and Floyd, 1977) and (c) MgO–FeOt–Na_2O+K_2O diagrams (after Irvine and Baragar, 1971) for the Neoproterozoic mafic rocks in the Central Jiangnan Orogen.

and Fig. 7a. Their measured $^{87}Sr/^{86}Sr$ ratios range from 0.71291 to 0.73344 and $^{143}Nd/^{144}Nd$ ratios from 0.51279 to 0.51362. When back-calculated to the formation age of 850 Ma, the corresponding initial $^{87}Sr/^{86}Sr$ ratios are in the range of 0.70796–0.71126 and $\varepsilon_{Nd}(t)$ values are from +1.30 to +9.36. The high initial $^{87}Sr/^{86}Sr$ ratios show a subhorizontal trend off the array of oceanic basalt (Fig. 7a), which could be caused by the isotopic exchange due to seawater hydrothermal alteration (e.g., Shuto et al., 2006; Fan et al., 2010).

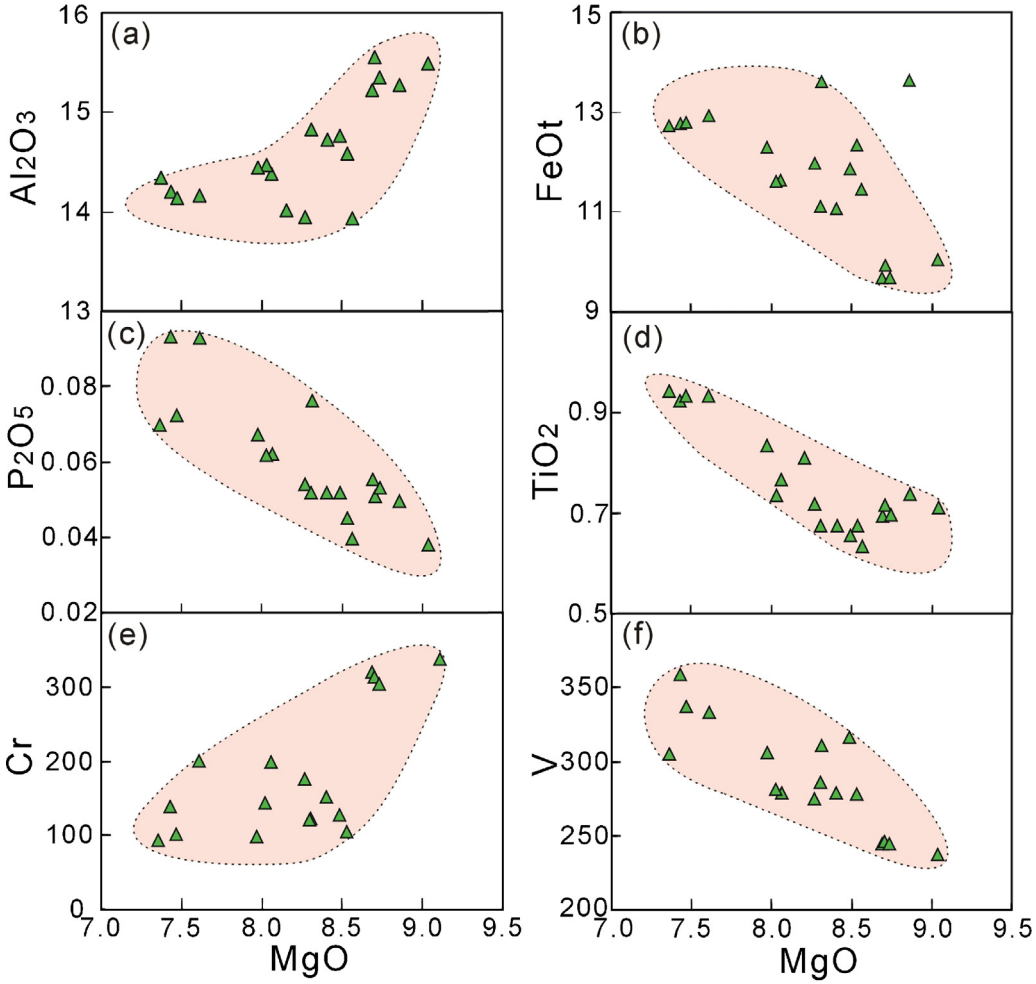

Fig. 5. Plots of MgO vs (a) Al_2O_3, (b) FeOt, (c) P_2O_5, (d) TiO_2, (e) Cr and (f) V vs MgO for the Neoproterozoic mafic rocks in the Central Jiangnan Orogen.

6. Discussion and tectonic implications

6.1. Formation age of the mafic lava in the Lengjiaxi Group

The geochronological data have been poorly reported for the mafic rocks along the Central Jiangnan Orogen, with the exception of a $^{207}Pb/^{206}Pb$ evaporation age of 1271 ± 2 Ma for the Nanqiao basalt reported by Zhou et al. (2003). Our dating grains from three samples (09WS-1, 09WS-3A and 10WS-10) mostly show weak oscillatory zoning and high Th/U ratios, the typical characteristics of a magmatic origin. They yield the weighted mean ages of 860 ± 20 Ma (n = 7, Shuikou basalt), upper intercept age of 847 ±18 Ma (n = 25, Fangxi dolerite) and the apparent $^{206}Pb/^{238}U$ age of 838 ±12 Ma (n = 1, Nanqiao basalt), respectively.

Numerous geochronological data show that the detrital zircons from the sandy rocks in the middle-upper segment of the Lengjiaxi Group and its equivalents (Sibao, Fanjinshan and Shuangqiaoshan Groups) have the youngest age-cluster at ~860–880 Ma (e.g., Wang et al., 2007, 2012d; Zhou et al., 2009; Zhao et al., 2011). This places a constraint on the maximum deposition age of 860–880 Ma for the majority of the exposed Lengjiaxi Group. The bentonite, tuff and dacite from the exposed Lengjiaxi Group and its equivalents give the zircon U–Pb ages ranging from 831 Ma to 850 Ma (Gao et al., 2008, 2010; Dong et al., 2010; Wang et al., 2006; Zhao et al., 2011; Zhou et al., 2009). The intermediate-acid volcanic sequence with a high-mg geochemical affinity, which is underlain by the Lengjiaxi Group but overlain by the Banxi Group, were dated at 822–824 Ma (Zhang et al., 2012b). In addition, the granitic plutons (e.g., Jiuling, Xiyuankeng) that intruded the Lengjiaxi and Shuangqiaoshan Groups have the crystallization ages of 804–823 Ma (Fig. 1b; e.g., Ma et al., 2009; Li et al., 2003; Zhang et al., 2011a). As introduced above, the tholeiitic mafic lava occurred as interlayer in the Lengjiaxi and Shuangqiaoshan packages (Fig. 2a and b). Synthesis of these age data and their spatial relationship suggests that the deposition timing of the exposed Lengjiaxi Group in NE Hunan and the Shuangqiaoshan Group in west Jiangxi should be older than ~822 Ma and the majority be younger than ~860 Ma. Thus, the age of 847 ± 18 Ma from the Fangxi dolerite is reliable, and the ages of 838 Ma and 860 Ma from the Shuikou and Nanqiao basalts can be used as the reference ages, suggesting that the eruption age of the mafic lava along the Central Jiangnan Orogen is ~850 Ma. In addition, a part of the grains from 09WS-3A and 10WS-10 gives an age-cluster of ~1800 Ma, representing the age of the xenolithic zircons. This probably suggests the development of the Paleoproterozoic basement beneath the Central Jiangnan Orogen in spite of poor outcrops. The previously-reported $^{207}Pb/^{206}Pb$ evaporation age of 1271 ± 2 Ma from the Nanqiao basalt probably represents a mixed age.

6.2. Origination from MORB source modified by arc component in the BAB setting

The samples analyzed in this study have experienced greenschist-facies metamorphism and have L.O.I. contents of

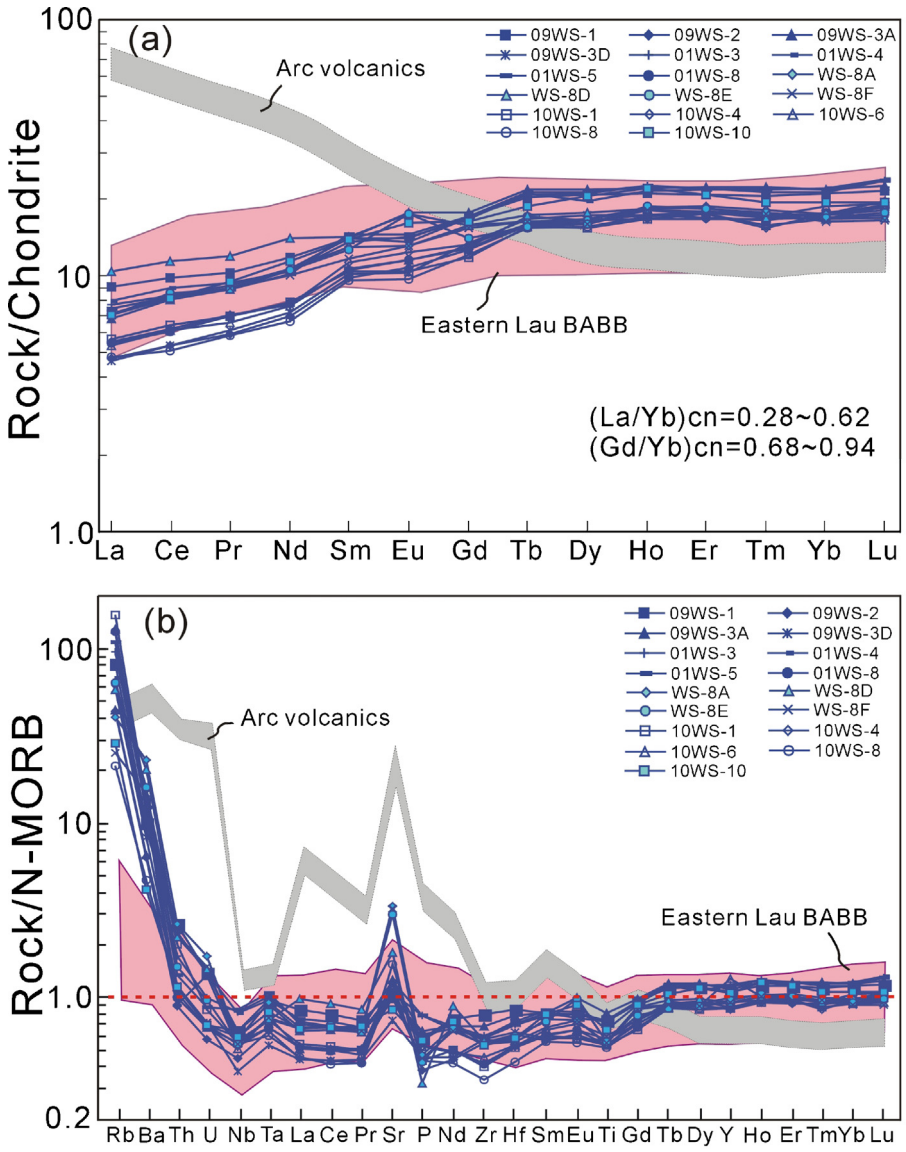

Fig. 6. The patterns of (a) the chondrite-normalized rare-earth elements, and (b) N-MORB-normalized spidergram for the Neoproterozoic mafic rocks along the Central Jiangnan Orogen. Normalized values for chondrite and N-MORB are from Sun and McDonough (1989). Also shown are the patterns for the eastern Lau BABB (Tian et al., 2008) and arc volcanics (Luhr and Haldar, 2006).

1.76–3.37 wt%, showing weak weather alteration. Discussion of petrogenesis herein focuses on the high field strength elements, which are considered least susceptible to metamorphism and alteration (e.g., Nb, Ta, Zr, Hf, REE, Th, Ti, Y, V and Sc) rather than those that are considered to be more mobile (e.g. Rb, Sr, K; Pearce, 1975; Wood et al., 1979).

These samples have the mg-number from 57 to 68, reflective of certain degree of the fractionation crystallization of the olivine and clinopyroxene. It is also noted that Cr concentration decreases but V increases remarkably with magma evolution (Fig. 5e and f). This provides additional evidence for clinopyroxene fractionation from the parental magma. Weak Eu anomalies (Fig. 6b) and positive correlation between MgO and Al_2O_3 (Fig. 5a) probably indicate poor fractionation of plagioclase. However, on the plot of La and La/Sm, these samples plot along the trend of source heterogeneity or dynamic melting rather than that of the fractionation crystallization (Fig. 7b). It is apparent that a petrogenetic model of simple fractionation can not fully explain the variety of incompatible element ratios (e.g., Nb/La of 0.54–1.12) and isotopic compositions ($\varepsilon_{Nd}(t)$ of 1.30–9.36).

The relatively constant Nb/La ratios and highly positive $\varepsilon_{Nd}(t)$ values irrespective of MgO suggest an insignificant crustal assimilation (Fig. 8a). The samples with high MgO contents have lower $\varepsilon_{Nd}(t)$ values than those with low MgO content (Fig. 8b). For example, the sample (WS-8D) with the highest MgO (9.04 wt%) shows mg-number of 68, slightly lower than that of the primary magma, but has the lowest $\varepsilon_{Nd}(t)$ values (+1.30) and relatively low Nb/La ratio (0.54). The sample (01WS-3) with the lowest MgO content has $\varepsilon_{Nd}(t)$ value of up to +8.21 (Table 2). The samples with low MgO contents exhibit higher Fe_2O_3 content relative to the high MgO samples (Fig. 4b). More importantly, our samples are characterized by the depletion in LREE relative to HREE and the lower contents of highly incompatible elements (from U to Ti) than those of N-MORB source (Fig. 6a and b). When significant crustal contamination en route is considered, at least 20–70% SCB crustal materials are required to be involved in the mantle-derived magma to balance the observed variations in Nb/La ratios. Such high-proportional addition of crust materials is obviously impossible for maintaining the basaltic compositions and balancing the Sr–Nd isotopic ratios of these samples.

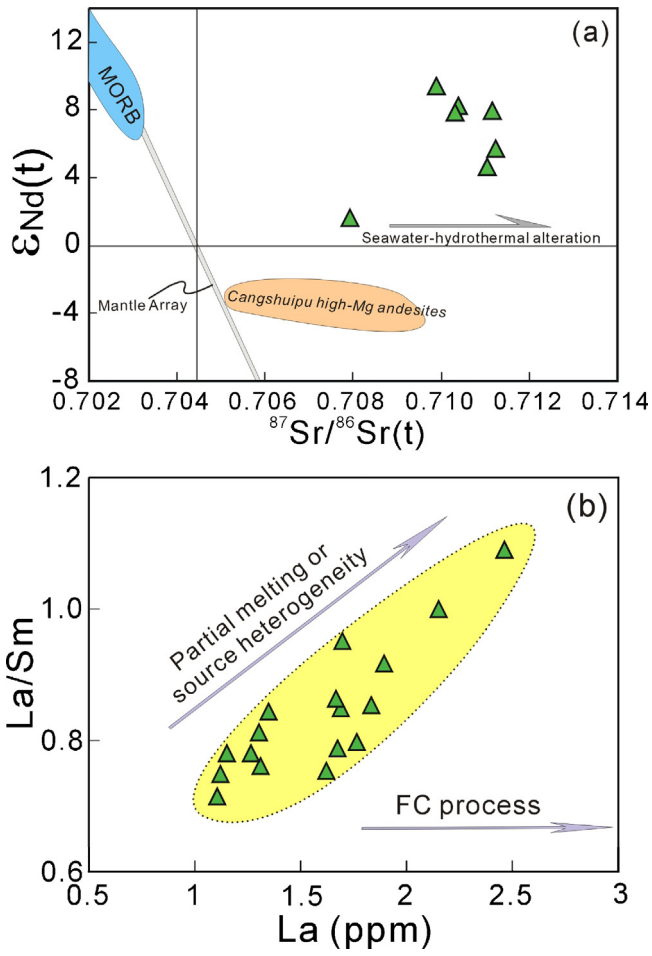

Fig. 7. Plots of (a) initial $^{87}Sr/^{86}Sr$ (t) vs $\varepsilon_{Nd}(t)$ (t = 850 Ma) and (b) La vs La/Sm for the Neoproterozoic mafic rocks in the Central Jiangnan Orogen. The fields of MORB, mantle array and Cangshuipu high-mg andesites are from Zimmer et al. (1995), Zhou et al. (2006) and Zhang et al. (2012b), respectively.

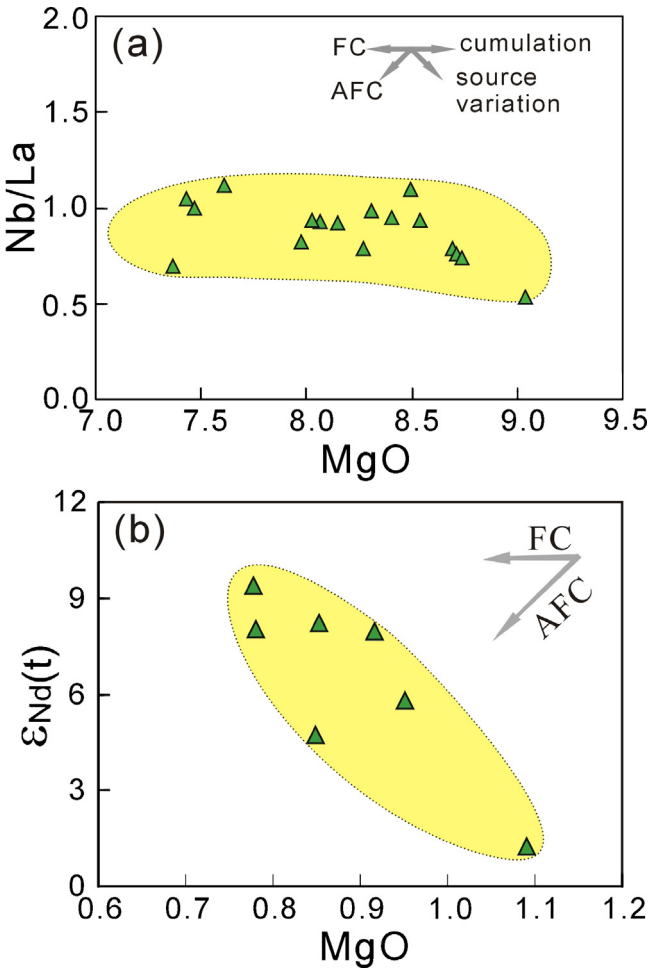

Fig. 8. Plots of MgO vs (a) Nb/La and (b) $\varepsilon_{Nd}(t)$ for the Neoproterozoic mafic rocks in the Central Jiangnan Orogen.

Such signatures, together with the presence of the xenocrystic zircons in our samples, suggest that the crustal contamination en route is most likely very weak and insufficient to change their elemental and isotopic compositions.

The chondrite-normalized REE patterns are strongly depleted in the LREE compared with HREE (Fig. 6a), suggesting an affinity to an N-MORB source. The N-MORB-normalized patterns for these samples are characterized by relative enrichment in very highly incompatible elements (e.g., Rb, Ba and Th) and depletion in highly incompatible elements (e.g., Nb, La, Ce, Zr, Sm and Eu). The pattern for moderately incompatible elements (e.g., Tb, Dy, Y, Yb and Lu) is generally similar to that of the N-MORB (Fig. 6b). In addition, the Nb/Ta (11–16) and Nb/Yb (0.30–0.54) ratios are lower than those of N-MORB (17 and 0.76, respectively). All these patterns suggest a derivation from more refractory mantle source relative to average N-MORB (Fig. 9a). Similar consideration is given in the plot of Fe8 vs Na8 Fe8 (Fig. 9b), in which the majority of these samples fall into the region below the MORB global trend. However, these samples have higher Th contents, and lower Th/Yb (0.04–0.11) and Th/Zr (0.003–0.008) ratios than those of average N-MORB (0.12 ppm, 0.04, 0.002, respectively (e.g., Sun and McDonough, 1989; Kepezhinaskas et al., 1996; Lapierre et al., 2000; Kerr et al., 2002). Their Th/La ratios range from 0.08 to 0.19, falling between those of bulk continental crust (~0.3) and N-MORB (0.05) (e.g., Hoffman and Ranalli, 1988; Sun & McDonough, 1989). In Fig. 9a, the increase of Th/Yb ratios with Nb/Yb ratios plots above the depleted back-arc line across the N-MORB and implies that these samples have experienced an subduction-related enrichment process. In Fig. 10a–c, these samples bridge the regions of the MORB and arc-volcanics.

In the $\varepsilon_{Nd}(t)$-Nb/La and Nb/Zr–Th/Zr Nb/diagrams (Fig. 11a and b), a mixed trend is well defined, suggesting the involvement of two end-members in the magma source without the consideration of the crustal contamination en route. One end-member is characterized by high $\varepsilon_{Nd}(t)$ (>9.0) and Nb/La (>1.0) but low Nb/Zr (<0.03) and Th/Zr (<0.002), resembling those of average N-MORB. The other most likely has a geochemical affinity to arc volcanics with $\varepsilon_{Nd}(t)$ <1.0, Nb/La <0.5, Nb/Zr >0.06 and Th/Zr >0.01. The input of the arc-component is further evidenced by the low Ti/V ratios (12–18) and TiO_2 (0.62–0.92 wt%) contents for these samples, which fall into the field of arc tholeiite in the Zr–Ti diagram (Fig. 10c). Such arc-like elemental signatures, together with their lower Nb/U (16–45) and Ce/Pb (0.4–2.5) ratios and highly positive $\varepsilon_{Nd}(t)$ values, suggest the involvement of an arc-like component in the MORB-like source. Therefore, the first-order interpretation is that these mafic samples have a depleted MORB-like source with an addition of a "crustal" component released from the subducted slab or sediment at the convergent margin (e.g., McCulloch and Gamble, 1991; Pearce and Peate, 1995; Shinjo et al., 1999).

The question remains as to which component (c.f. slab- and sediment-derived components) is newly added into the source. An analysis combining Nd/Pb and Nb/Y ratios with isotope compositions can effectively evaluate the nature of subduction components, because Nd, Nb and Y contents are generally dominated by

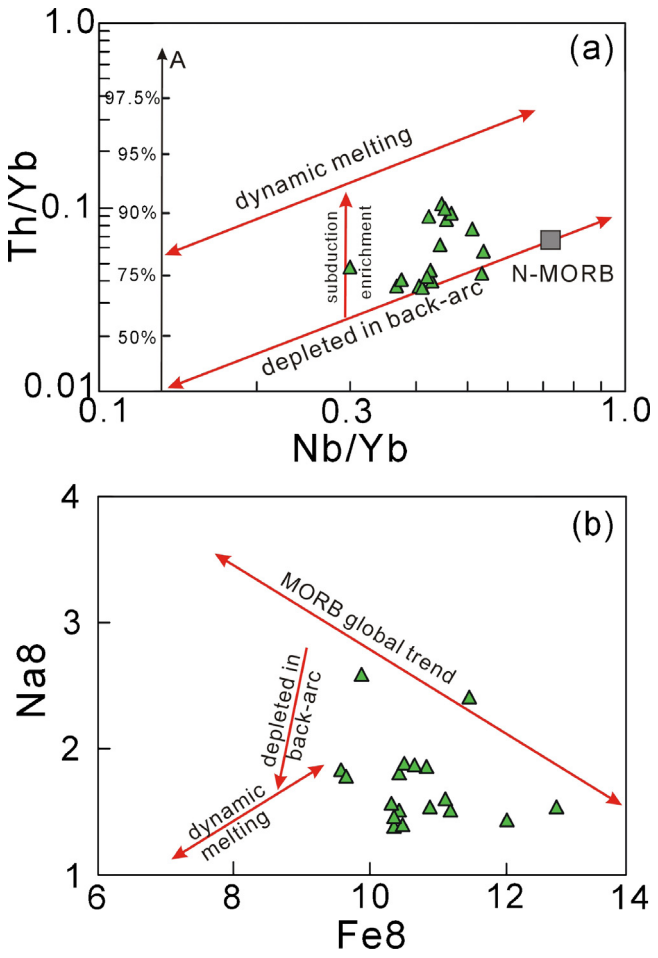

Fig. 9. Plots of (a) Nb/Yb vs Th/Yb (after Pearce et al., 1995), and (b) Fe8 vs Na8 (after Pearce et al., 1995) for the Neoproterozoic mafic rocks in the Central Jiangnan Orogen.

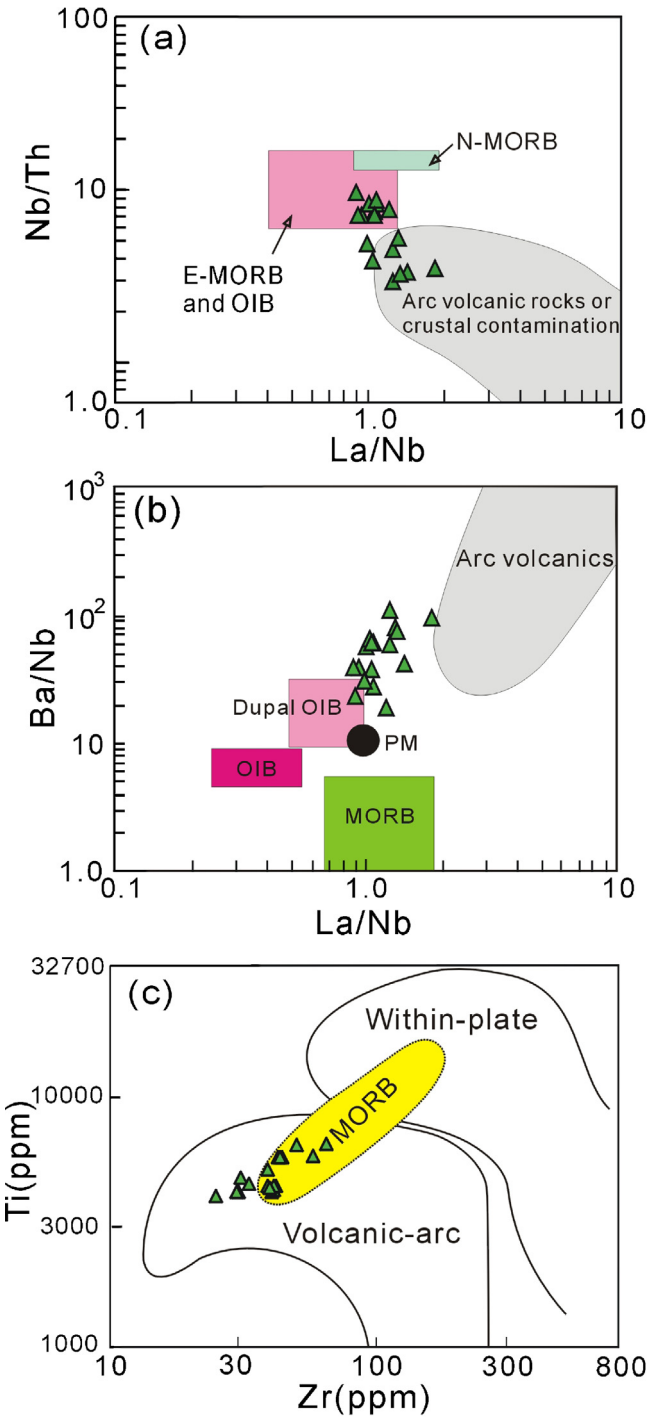

Fig. 10. Plots of (a) La/Nb vs Nb/Th, (b) La/Nb vs Ba/Nb (after Fan et al., 2004), and (c) Zr vs Ti (after Pearce, 1982) for the Neoproterozoic mafic rocks in the Central Jiangnan Orogen.

sediment- and slab-derived melts but Pb is controlled by hydrous fluids formed by dehydration of the oceanic crust as a result of distinct mobility of these elements (e.g., Brenan et al., 1995a, 1995b; Elliott et al., 1997; Kogiso et al., 1997; Castillo et al., 2002, 2007; Castillo, 2008; Class et al., 2000; Petrone and Ferrari, 2008). Our samples show lower Nd/Pb ratios (0.40–2.51) than those of typical MORB mantle (~24) and plot along the mixed line of the mantle wedge modified by fluids and subducted sediment in Nd/Pb vs $\varepsilon_{Nd}(t)$ diagram (Fig. 11c). The weak changes of Th/Yb ratios irrespective of Ba/La ratios also argue for the flux of fluids. In Fig. 11d, they plot along the mixed line of a MORB source (or mantle wedge modified by slab-derived fluid) with the subducted sediment-derived melt (e.g., Gertisser and Keller, 2003; Seghedi et al., 2004; Class et al., 2000; Petrone and Ferrari, 2008). In the Harker diagram (Fig. 5), Al_2O_3 correlates positively but FeOt negatively with MgO, indicating that the magma source is characterized by high Al_2O_3 and low FeOt. These, taking into account the high $\varepsilon_{Nd}(t)$ values for our samples, probably suggest the small-proportional involvement of a recycled sedimentary component. The synthesis of all these data indicates the magma source of these samples has subjected to a joint modification by the flux of the slab-derived fluid and proportional input of the recycled sediment-derived melt.

The input of such "crustal" component suggests that the mafic rocks in the Central Jiangnan Orogen might be related to a subduction rather than a spreading oceanic setting (e.g., Zhou et al., 2003). In the Th–Hf–Ta and Zr–Nb–Y discriminated diagrams (Fig. 12a and b), these samples plot into the field of N-MORB and volcanic-arc basalts. Their geochemical affinity to both MORB- and arc-like components might be genetically related to the fore-arc or back-arc basin settings (e.g., Hawkins, 1995; Shinjo et al., 1999; Sandeman et al., 2006; Teklay, 2006). However, there are little evidence or poor reports for supporting the development of the contemporaneous boninite, high-mg andesite and arc-andesite along the Central Jiangnan Orogen so far, inconsistent with what would be expected for the rocks association in a fore-arc basin setting (e.g., Hawkins, 1995; Gribble et al., 1998; Shinjo et al., 1999; Shuto et al., 2006; Rolland et al., 2009). Moreover, our samples have similar (La/Yb)n,

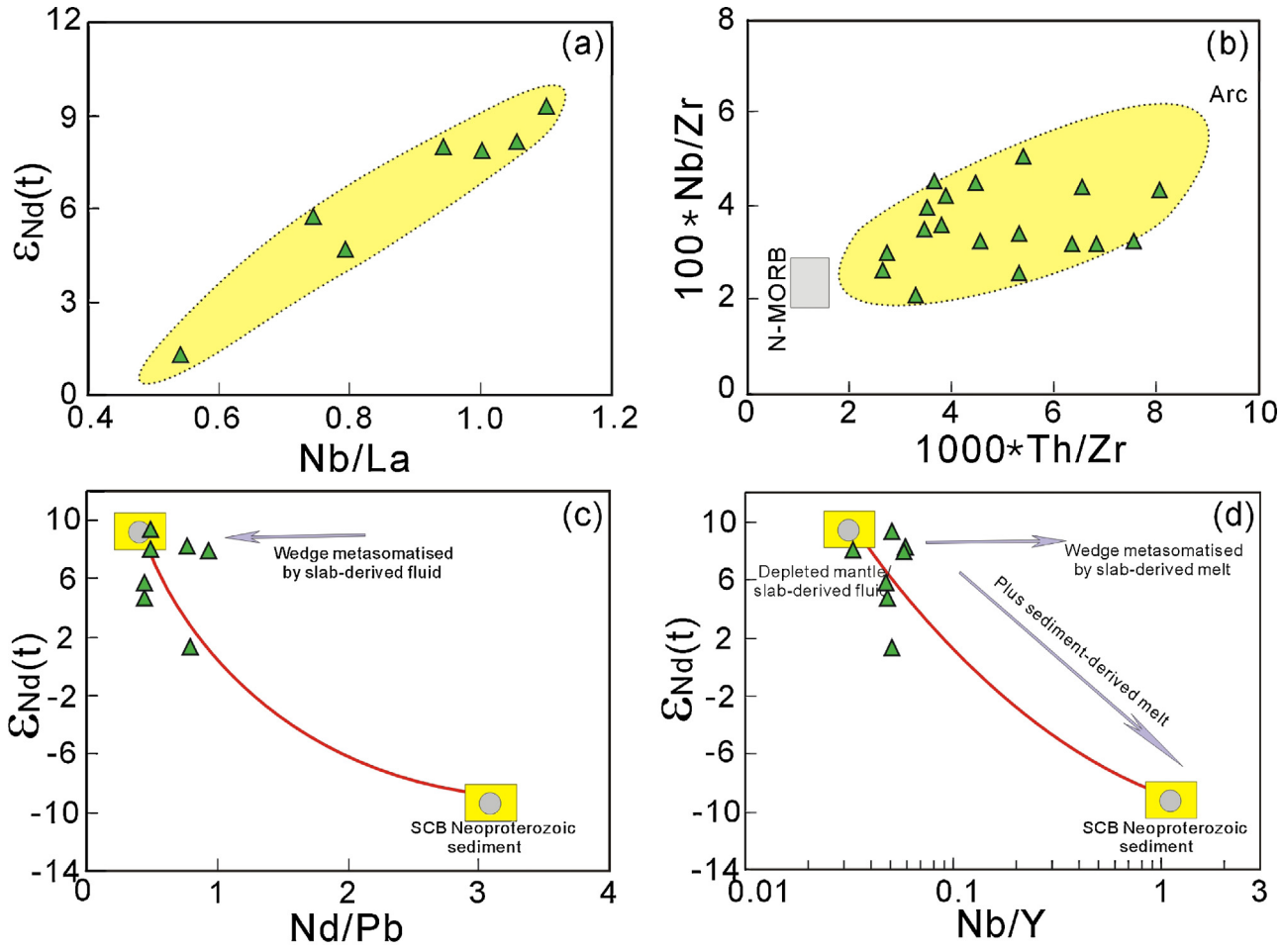

Fig. 11. Plots of (a) Nb/La vs $\varepsilon_{Nd}(t)$ (t), (b) 1000*Th/Zr vs 100*Nb/Zr, (c) Nd/Pb vs $\varepsilon_{Nd}(t)$, and (d) Nb/Y vs $\varepsilon_{Nd}(t)$ for the Neoproterozoic mafic rocks in the Central Jiangnan Orogen. The compositions of the end-members are from Elliott et al. (1997), Class et al. (2000), Petrone and Ferrari (2008), Castillo et al. (2002, 2007) and Wang et al. (2003b, 2011b, 2013).

Sm/Nd, Th/Yb and Th/Nb ratios, as well as REE and multi-elemental patterns to those in Eastern Lau Basin, typical of the modern back-arc basin (Fig. 6a and b, Tian et al., 2008). They fall into the range of the back-arc basin basalt in Fig. 12c. On the plot of Th/Nb vs Ce/Nb (Fig. 12d), these samples plot into the field of the Japan Sea back-arc basin that initiated in the rifting of continental crust (e.g., Pouclet et al., 1995; Shuto et al., 2006; Sandeman et al., 2006; Emilio et al., 2011). Low Nb/Ta ratios (11–16) in arc-lavas are also commonly regarded as indicative of a mantle wedge which is the residual to the back-arc melting (e.g., Class et al., 2000). In addition, the trends in Fig. 10a and b for these samples reflect that the formation of the mafic lava is related to the subduction enrichment after the previous melt extraction in a back-arc setting. The previous melt extraction might result in stronger depletion in very high and high incompatible elements than moderately incompatible elements in the mantle source, and lower Na8 relative to Fe8, due to the loss of a small melt fraction. During subduction enrichment, the subducted component would lead to high Ba/Nb and Th/Yb ratios due to its high proportions of Rb, Ba and Th in the depleted source. Such processes are operating most likely in the back-arc basin setting (e.g., Pearce and Peate, 1995; Emilio et al., 2011). Samples 09WS-3A and 10WS-10 preserved abundant xenolithic zircons with the ages grouping at ~1800 Ma and ~2500 Ma. These ages reflect the presence of the continental basement prior to volcanic eruption at ~850 Ma. Therefore, it can be concluded that the mafic rocks developed in a continental back-arc basin along the central Jiangnan Orogen at ~850 Ma.

6.3. Amalgamation along the Central Jiangnan Orogen and its eastward extension

The formation of the SCB is commonly considered as the result of the amalgamation of the Yangtze with Cathaysia Blocks. The Jiangnan Orogen is traditionally interpreted as the suture of the oceanic subduction and subsequent collisional orogen between the Yangtze and Cathaysia Blocks in spite that different amalgamation times have been proposed (~880 Ma vs ~820 Ma vs ~800 Ma; e.g., Li et al., 1995, 2002, 2008a, 2009a; Ye et al., 2007; Wang et al., 2006, 2007, 2008a, 2008b; Zheng et al., 2007; Zhao et al., 2011; Zhang et al., 2012b and reference therein).

Our data demonstrate that there occurred a ~850 Ma back-arc basin in the Wenjiashi-Fangxi areas of the Central Jiangnan Orogen. In the Fuchuan area in south Anhui Province, the gabbro and wehrlite in ophiolite suite yielded the zircon U–Pb ages of 848 ± 12 Ma and 827 ± 9 Ma, respectively (Ding et al., 2008). Zhang et al. (2012a) obtained a zircon U–Pb age of 824 ± 3 Ma from the gabbro in the Fuchuan ophiolite with the geochemical affinity to the back-arc basin. In the Zhangyuan (NE Jiangxi) and Leigongcao (NW Jiangxi) areas, synchronological pillow basalt and spilite with similar geochemical signatures have also been identified (Zhang et al., 2011b, 2012b and authors' unpublished data). These signatures indicate the development of the 824–860 Ma back-arc basin along the Wenjiashi-Fangxi and Fuchuan-Zhangyuan areas, with a closure time later than ~830 Ma. Field observations show that the greywacke-slate-schist-tuff Banxi Group (and its

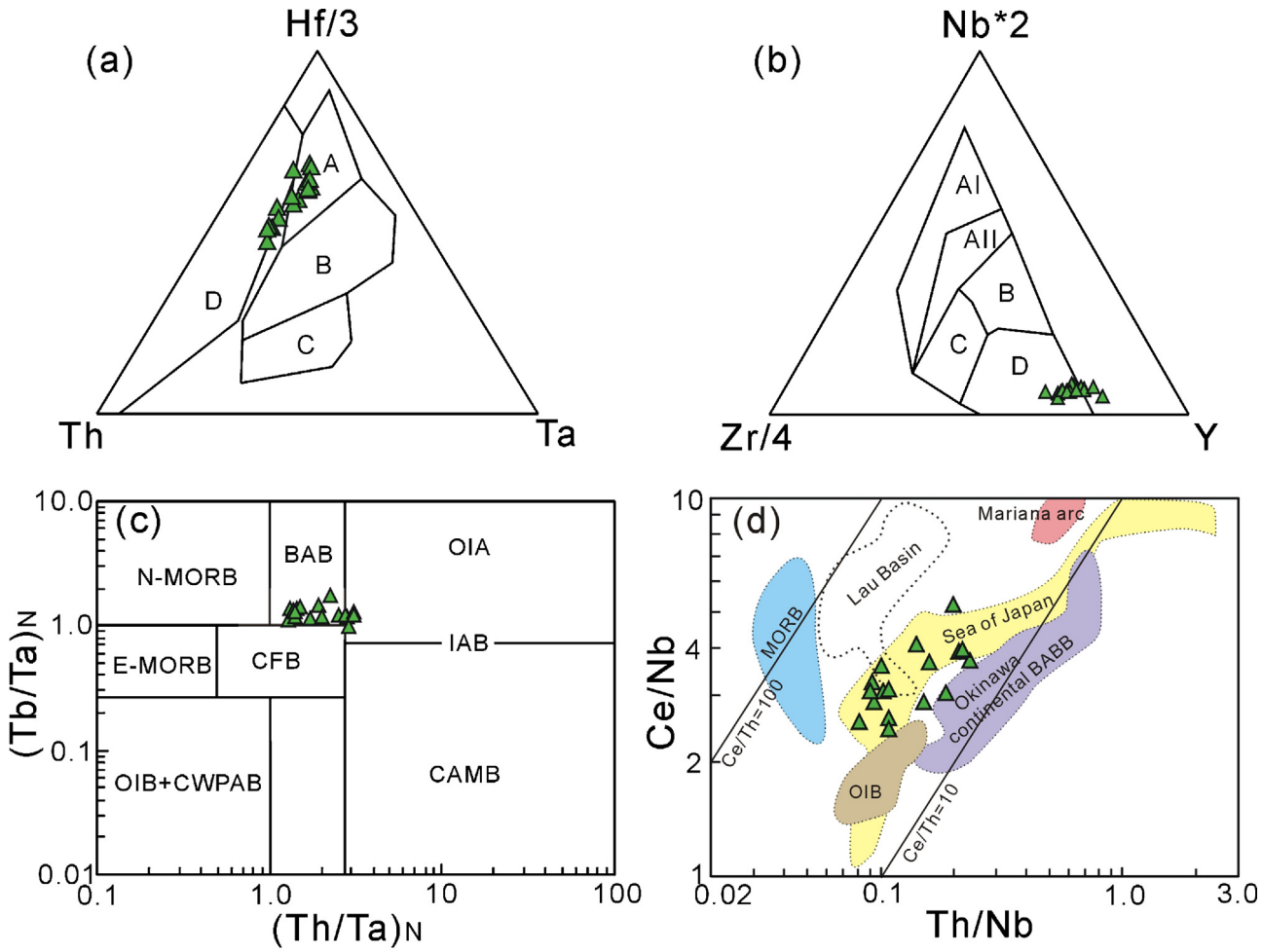

Fig. 12. (a) Th-Hf-Ta diagram (after Wood, 1980), (A) N-MORB, (B) E-MORB and within-plate tholeiites, (C) alkaline within-plate basalts and (D) volcanic-arc basalts. (b) Zr–Nb–Y diagram (after Meschede, 1986), (AI) within-plate alkali basalts (AII) within-plate alkali basalts and within-plate tholeiites, (B) E-MORB, (C) within-plate tholeiites and volcanic-arc basalts, (D) N-MORB and volcanic-arc basalts. (c and d) Plots of $(Th/Ta)_N$ vs $(Tb/Ta)_N$ (after Fekkak et al., 2001) and Th/Nb Ce/Nb vs Ce/Nb Th/Nb (after Taylor and Martinez, 2003) for the Neoproterozoic mafic rocks in the Central Jiangnan Orogen. N-MORB: "normal" MORB, E-MORB: enriched MORB, BAB: back-arc basin basalts, CFB: continental flood basalts, OIA: Mariana-type intra-oceanic arc, IAB: intermediate arc basalts, OIB: ocean island basalts, CWPAB: continental within-plate alkali and transitional basalts; and CAMB: active continental margin basalts.

equivalents) deposited in the failed-rift setting and overlies the abysmal flysch- and turbidite-facies Lengjiaxi Group (and its equivalents) with an angular unconformity (e.g., Hunan BGMR, 1988; Jiangxi BGMR, 1984). In the Cangshuipu area of the Central Jiangnan Orogen, below the angular unconformity marked by a conglomerate layer, there occurred the Yinzhuba high-mg volcanic agglomerates dated at 822–824 Ma (e.g., Pan, 2001; Zhang et al., 2012b). The tuff, bentonite and volcanic interlayer from the Banxi Group (and its equivalents) gave the zircon U–Pb ages of 719–809 Ma (Wang et al., 2008b, 2012a, 2012b; Gao et al., 2008, 2010; Yin et al., 2003; Zhang et al., 2008; Chen et al., 2005; Wu et al., 2007; Zheng et al., 2008; Huang et al., 2009). The oldest granite intruding the Banxi Group at Chengbu (western Hunan Province) was dated at 806 ± 9 Ma (Bai et al., 2010). These data constrain the final amalgamation of the Yangtze and Cathaysia Blocks along the Central Jiangnan Orogen being at ~806–822 Ma.

Previous studies (e.g. Xu et al., 1992; Charvet et al., 1996) suggested that the Zhangshudun ophiolite in NE Jiangxi and the Fuchuan ophiolite in South Anhui belong to the same ophiolite suite, representing the suture boundary of the Yangtze and Cathaysia Blocks along the Eastern Jiangnan Orogen (Fig. 1a). However, in the Shuangxiwu area of NE Zhejiang and the Zhangshudun area of NE Jiangxi, there preserved the SSZ-type ophiolite suite, arc-like volcanic rocks, subduction-related granites and adakites, which were dated at 900–970 Ma (e.g., Chen et al., 1991; Li et al., 1994, 2008a, 2009a; Li and Li, 2003; Wu et al., 2006; Ye et al., 2007). The associated plagiogranite, andesite, amphibolite-bearing tonalite and granodiorite yielded the zircon U–Pb ages of 900–930 Ma and show an arc-like geochemical affinity with positive $\varepsilon_{Nd}(t)$ and $\varepsilon_{Hf}(t)$ values (e.g., Ye et al., 2007; Chen et al., 2009a,b; Li et al., 2009a). The glaucophane-bearing schist gave the metamorphic age of 866 ± 10 Ma (K–Ar method; Shu et al., 1993; Charvet et al., 1996). The Xiwan leucogranites and Zhangcun rhyolite in the Zhangshudun ophiolitic suite, interpreted as anatexis product of arc-derived sedimentary materials, were dated at 880 ± 19 Ma and 891 ± 19 Ma, respectively (e.g., Li et al., 2008a, 2009a). These data are synthetically interpreted as indicating the development of intra-oceanic arc at ~900–970 Ma and possible amalgamation at ~880 Ma along the Zhangshudun and Shuangxiwu areas. It is obvious that the igneous magmatism along the Zhangshudun-Shuangxiwu areas is significantly older than that along Central Jiangnan Orogen and Fuchuan in South Anhui (e.g., Ye et al., 2007; Li et al., 2008a, 2009a; Chen et al., 2009a,b). Therefore, the Fuchuan and Zhangshudun ophiolites might be two different ophiolite suites formed at different time during Neoproterozoic amalgamation in Eastern South China. Such a temporal and spatial

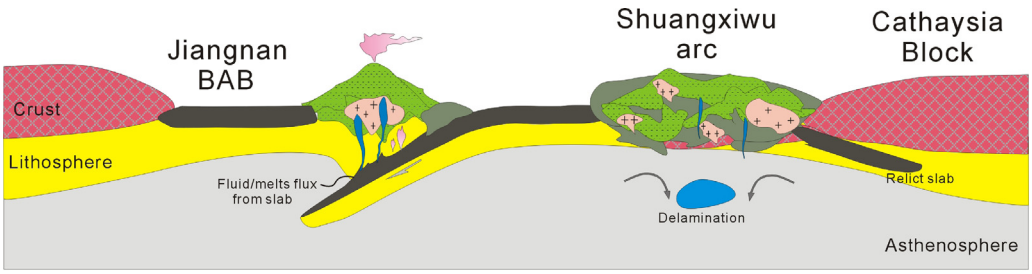

Fig. 13. Schematic cartoon showing the tectonic pattern at ~830–860 Ma across the Jiangnan back-arc basin and Shuangxiwu arc.

relationship shows that the Central Jiangnan Orogen links easterly to the Zhangyuan-Fuchuan area along the Jingdezhen fault rather than toward the Zhangshudun-Shuangxiwu area along the Jiangshan-Shaoxing fault (Wang et al., in press).

In summary, our data synthesis suggests that the amalgamation regime along the central Jiangnan Orogen and Zhangyuan-Fuchuan areas (renamed eastern Jiangnan orogen) contributed to the closure of the back-arc basin rather than oceanic subduction (Zheng, 2012; Zheng et al., 2013; Zhang et al., 2012a) This supports the model of the Neoproterozoic orogenism in the eastern SCB might be characterized by arc-collision accretion assembly as a part of an exterior accretionary orogen along the periphery of Rodinia. This consideration is further supported by the following observations: (1) poor occurrence of synchronous low temperature and high pressure metamorphism; and (2) ~800–830 Ma peraluminous granite characterized by positive $\varepsilon_{Hf}(t)$ values (juvenile component) and high $\delta^{18}O$ values (e.g., Wu et al., 2006; Zhang et al., 2011a; Ma et al., 2009). Based on all the available geological, geochemical and geochronological data, we suggest a cartoon for the tectonic pattern at ~830–860 Ma across the Jiangnan back-arc basin and Shuangxiwu arc (Fig. 13). This may give us a hint that accretionary orogens are characterized by multiple accretionary orogenic processes, including the following stages of (1) the Shuangxiwu arc being accreted to the Cathaysia Block at ~880 Ma (e.g., Ye et al., 2007; Li et al., 2008a, 2009a; Chen et al., 2009a,b), and (2) the closure of the short-aged back-arc basin (830–860 Ma) by ~820 Ma orogenic event along Jiangnan Orogen (Zhang et al., 2012a,b; Wang et al., 2008b, 2012a, 2012b; Gao et al., 2008, 2010 and authors' unpublished data).

Acknowledgements

We would like to thank C-H Zhang and T-P Peng for their help during field work and samples collection. We are grateful to G-C Zhao and two anonymous reviewers for their critical and constructive review and comment on this paper. This study was jointly supported by the China Natural Science Foundation (40825009 and 41190073), State Key Laboratory of Ore Deport Geochemistry, Chinese Academy of Sciences (201301) and the Chinese Academy of Sciences (GIGCAS-135-Y234151001). This is a contribution to Guangzhou Institute of Geochemistry, the Chinese Academy of Sciences.

References

Bai, D.Y., Jia, B.H., Liu, W., Chen, B.H., Liu, Y.R., Zhang, X.Y., 2010. Zircon SHRIMP U–Pb dating of the igneous rocks from Chengbu, Hunan: constraint on the Neoproterozoic tectonic evolution of the Jiangnan Orogenic Belt. Acta Geologica Sinica 12, 1715–1726 (in Chinese with English Abstract).

Brenan, J.M., Shaw, H.F., Ryerson, F., 1995a. Experimental evidence for the origin of lead enrichment in convergent-margin magmas. Nature 378, 54–56.

Brenan, J.M., Shaw, H.F., Ryerson, F.J., Phinney, D.L., 1995b. Mineral-aqueous fluid partitioning of trace elements at 900 °C and 2.0 GPa: constraints on the trace element chemistry of mantle and deep crustal fluids. Geochimica et Cosmochimica Acta 59, 3331–3350.

Castillo, P.R., 2008. Origin of the adakite-high-Nb basalt association and its implications for post-subduction magmatism in Baja California, Mexico. Geological Society of American Bulletin 120, 451–462.

Castillo, P.R., Solidum, R.U., Punogbayan, R.S., 2002. Origin of high field strength element enrichment in the Sulu Arc, southern Philippines, revisited. Geology 30, 707–710.

Castillo, P.R., Rigby, S.J., Solidum, R.U., 2007. Origin of high field strength element enrichment in volcanic arcs: geochemical evidence from the southern Sulu Arc, southern Philippines. Lithos 97, 271–288.

Charvet, J., Shu, L.S., Shi, Y.S., Guo, L.Z., Faure, M., 1996. The building of South China: collision of Yangzi and Cathaysia blocks, problems and tentative answers. Journal of Southeast Asian Earth Science 13 (3–5), 223–235.

Chen, J.F., Foland, K.A., Xing, F.M., Xu, X., Zhou, T.X., 1991. Magmatism along the southeast margin of the Yangtze block: precambrian collision of the Yangtze and Cathysia blocks of China. Geology 19, 815–818.

Chen, J.F., Jahn, B.M., 1998. Crustal evolution of Southeast China: Nd and Sr isotopic evidence. Tectonophysics 284, 101–133.

Chen, Y.L., Luo, Z.H., Zhao, J.X., Li, Z.H., Zhang, H.F., Song, B., 2005. Petrogenesis and dating of the Kangding complex, Sichuan Province. Science in China Series D: Earth Sciences 48 (5), 622–634.

Chen, Z.H., Guo, K.Y., Dong, Y.G., Chen, R., Li, L.M., Liang, Y.H., Li, C.H., Yu, X.M., Zhao, L., Xing, G.F., 2009a. Possible early Neoproterozoic magmatism associated with slab window in the Pingshui segment of the Jiangshan-Shaoxing suture zone: evidence from zircon LA-ICP-MS U–Pb geochronology and geochemistry. Science in China Series D: Earth Science 52 (7), 925–939 (in Chinese with English Abstract).

Chen, Z.H., Xing, G.F., Guo, K.Y., Dong, Y.G., Chen, R., Zeng, Y., Li, L.M., He, Z.Y., Zhao, L., 2009b. Petrogenesis of keratophyes in the Pingshui Group, Zhejiang: constraints from zircon U–Pb ages and Hf isotopes. Chinese Science Bulletin 54 (5), 610–617 (in Chinese with English Abstract).

Class, C., Miller, D.M., Goldstein, S.L., Langmuir, C.H., 2000. Distinguishing melt and fluid subduction components in Umnak Volcanics, Aleutian Arc. Geochemistry, Geophysics, Geosystems 1, 1004, http://dx.doi.org/10.1029/1999GC000010.

Compston, W., Williams, I.S., Meyer, C., 1984. U–Pb geochronology of zircons from Lunar Breccia 73217 using a sensitive high mass-resolution ion microprobe. Journal of Geophysical Research 89, B525–B534.

Ding, B.H., Shi, R.D., Zhi, X.C., Zheng, L., Chen, L., 2008. Neoproterozoic (~850 Ma) subduction in the Jiangnan orogen: evidence from the SHRIMP U–Pb dating of the SSZ-type ophiolite in southern Anhui Province. Acta Petrologica et Mineralogica 27 (5), 375–388 (in Chinese with English Abstract).

Dong, S.W., Xue, H.M., Xiang, X.K., Ma, L.C., 2010. The discovery of Neoproterozoic pillow lava in spilite-ceratophyre of Lushan area, northern Jiangxi Province, and its geological significance. Geology in China 37 (4), 1021–1033 (in Chinese with English Abstract).

Dong, Y.P., Liu, X.M., Santosh, M., Zhang, X.N., Chen, Q., Yang, C., Yang, Z., 2011. Neoproterozoic subduction tectonics of the northwestern Yangtze Block in South China: constrains from zircon U–Pb geochronology and geochemistry of mafic intrusions in the Hannan Massif. Precambrian Research 189, 66–90.

Dong, Y.P., Liu, X.M., Santosh, M., Chen, Q., Zhang, X.N., Li, W., He, D.F., 2012. Neoproterozoic accretionary tectonics along the northwestern margin of the Yangtze Block, China: constraints from zircon U–Pb geochronology and geochemistry. Precambrian Research 196–197, 247–274.

Elliott, T., Plank, T., Zindler, A., White, W., Bourdon, B., 1997. Element transport from slab to 678 volcanic front at the Mariana Arc. Journal of Geophysical Research 102 (14), 991–1015, 019.

Emilio, S., Luigi, B., Adonis, P., Ottavia, Z., 2011. Petrogenesis and tectono-magmatic significance of basalts and mantle peridotites from the Albanian–Greek ophiolites and sub-ophiolitic mélanges. New constraints for the Triassic–Jurassic evolution of the Neo-Tethys in the Dinaride sector. Lithos 124, 227–242.

Fan, W.M., Guo, F., Wang, Y.J., Zhang, M., 2004. Late Mesozoic volcanism in the northern Huaiyang tectono-magmatic belt, central China: partial melts from a lithospheric mantle with subducted continental crust relicts beneath the Dabie orogen? Chemical Geology 209, 27–48.

Fan, W.M., Wang, Y.J., Zhang, A.M., Zhang, F.F., Zhang, Y.Z., 2010. Permian arc–backarc basin development along the Ailaoshan tectonic zone: geochemical, isotopic and geochronological evidence from the Mojiang volcanic rocks, Southwest China. Lithos 119, 553–568.

Fekkak, A., Pouclet, A., Ouguir, H., Ouazzani, H., Badra, L., Gasquet, D., 2001. Geochemistry and geotectonic significance of Early Cryogenian

volcanics of Saghro (Eastern Anti-Atlas, Morocco). Geodinamica Acta 14, 373–385.
Gao, L.Z., Yang, M.G., Ding, X.Z., Liu, Y.X., Liu, X., Ling, L.H., Zhang, C.H., 2008. SHRIMP U–Pb zircon dating of tuff in the Shuangqiaoshan and Heshangzhen groups in South China—constraints on the evolution of the Jiangnan Neoproterozoic orogenic belt. Geological Bulletin of China 27, 1744–1751 (in Chinese with English Abstract).
Gao, L.Z., Dai, C.G., Liu, Y.X., Wang, M., Wang, X.H., Chen, J.S., Ding, X.Z., Zhang, C.H., Gao, C.Q., Liu, J.H., 2010. Zircon SHRIMP U–Pb dating of tuff bed of the Sibao Group in Southeastern Guizhou-Northern Guangxi area, China and its stratigraphic implication. Geological Bulletin of China 29, 1259–1267 (in Chinese with English Abstract).
Gao, L.Z., Chen, J., Ding, X.Z., Liu, Y.R., Zhang, C.H., Zhang, H., Liu, Y.X., Pang, W.H., Zhang, Y.H., 2011. Zircon SHRIMP U–Pb dating of the tuff bed of Lengjiaxi and Banxi groups, northeastern Hunan: constraints on the Wuling Movement. Geological Bulletin of China 30, 1001–1008 (in Chinese with English Abstract).
Gertisser, R., Keller, J., 2003. Temporal variations in magma composition at Merapi Volcano (Central Java, Indonesia): magmatic cycles during the past 2000 years of explosive activity. Journal of Volcanology and Geothermal Research 123, 1–23.
Gribble, R.F., Stern, R.J., Newman, S., Bloomer, S.H., O'Hearn, T., 1998. Chemical and isotopic composition of lavas from the Northern Mariana Trough: implications for magma genesis in back-arc–arc basins. Journal of Petrology 39, 125–154.
Hawkins, J.W., 1995. The geology of the Lau Basin. In: Taylor, B. (Ed.), Back-arc Basins: Tectonics and Magmatism. Plenum Press, New York, pp. 63–138.
Hoffman, P.F., Ranalli, G., 1988. Archean oceanic flack tectonics. Geophysical Research Letters 15 (10), 1077–1080.
Huang, X.L., Xu, Y.G., Lan, J.B., Yang, Q.J., Luo, Z.Y., 2009. Neoproterozoic adakitic rocks from Mopanshan in the western Yangtze Craton: partial melts of a thickened lower crust. Lithos 112, 367–381.
Hunan BGMR (Bureau of Geology and Mineral Resources of Hunan Province), 1988. Regional Geology of Hunan Province. Geological Publishing House, Beijing (in Chinese with English Abstract).
Irvine, T.N., Baragar, W.R.A., 1971. A guide to the chemical classification of the common volcanic rocks. Canada Journal of Earth Science 8, 523–548.
Jiangxi BGMR (Bureau of Geology and Mineral Resources of Jiangxi Province), 1984. Regional Geology of Jiangxi Province. Geological Publishing House, Beijing (in Chinese with English Abstract).
Kepezhinaskas, P.K., Defant, M.J., Drummond, M.S., 1996. Progressive enrichment of island arc mantle by melt–peridotite interaction inferred from Kamchatka xenoliths. Geochimica et Cosmochimica Acta 60, 1217–1229.
Kerr, A.C., Tarney, J., Kempton, P.D., Spadea, P., Nivia, A., Marriner, G.F., Duncan, R.A., 2002. Pervasive mantle plume head heterogeneity: evidence from the late Cretaceous Caribbean–Colombian oceanic plateau. Journal of Geophysical Research 107 (B7) (10.1029).
Kogiso, T., Tatsumi, Y., Nakano, S., 1997. Trace element transport during dehydration processes in the subducted oceanic crust: 1. Experiments and implications for the origin of ocean island basalts. Earth Planetary Science Letter 148, 193–205.
Lapierre, H., Bosch, D., Dupuis, V., Polvé, M., Maury, R., Hernandez, J., Monié, P., Yeghicheyan, D., Jaillard, E., Tardy, M., de Lepinay, B., Mamberti, M., Desmet, A., Keller, F., Senebier, F., 2000. Multiple plume events in the genesis of the peri-Caribbean Cretaceous oceanic plateau province. Journal of Geophysical Research 105, 8403–8421.
Li, W.X., Li, X.H., 2003. Adakitic granites within the NE Jiangxi ophiolite, South China: geochemical and Nd isotopic evidence. Precambrian Research 122, 29–44.
Li, W.X., Li, X.H., Li, Z.X., Lou, F.S., 2008a. Obduction-type granites within the NE Jiangxi Ophiolite: implications for the final amalgamation between the Yangtze and Cathaysia Blocks. Gondwana Research 13, 288–301.
Li, X.H., Zhou, G.Q., Zhao, J.X., Fanning, C.M., Compston, W., 1994. SHRIMP ion microprobe zircon U–Pb age of the NE Jiangxi ophiolite and its tectonic implications. Geochimica 23 (2), 125–131 (in Chinese with English Abstract).
Li, X.H., 1999. U–Pb zircon ages of granites from the southern margin of the Yangtze Block: timing of the Neoproterozoic Jinning Orogeny in SE China and implications for Rodinia Assembly. Precambrian Research, 43–57.
Li, X.H., Li, Z.X., Ge, W.C., Zhou, H.W., Li, W.X., Liu, Y., Wingate, M.T.D., 2003. Neoproterozoic granitoids in South China: crustal melting above a mantle plume at ca. 825 Ma? Precambrian Research 122, 45–83.
Li, X.H., Li, Z.X., Ge, W.C., Zhou, H.W., Li, W.X., Liu, Y., Wingate, M.T.D., 2004. Reply to the comment: mantle plume, but not arcrelated Neoproterozoic magmatism in South China. Precambrian Research 132, 405–407.
Li, X.H., Su, L., Chung, S.L., Li, Z.X., Liu, Y., Song, B., Liu, D.Y., 2005. Formation of the Jinchuan ultramafic intrusion and the world's third largest Ni–Cu sulfide deposit: associated with the ~825 Ma south China mantle plume? Geochemistry, Geophysics, Geosystems 6, Q11004, http://dx.doi.org/10.1029/2005GC 001006.
Li, X.H., Li, W.X., Li, Z.X., Lo, C.H., Wang, J., Ye, M.F., Yang, Y.H., 2009a. Amalgamation between the Yangtze and Cathaysia Blocks in South China: constraints from SHRIMP U–Pb zircon ages, geochemistry and Nd–Hf isotopes of the Shuangxiwu volcanic rocks. Precambrian Research 174, 117–128.
Li, X.H., Liu, Y., Li, Q.L., Guo, C.H., Chamberlain, K.R., 2009b. Precise determination of Phanerozoic zircon Pb/Pb age by multi-collector SIMS without external standardization. Geochemistry, Geophysics, Geosystems 10, Q04010, http://dx.doi.org/10.1029/2009GC002400.
Li, X.H., Li, W.X., Li, Q.L., Wang, X.C., Liu, Y., Yang, Y.H., 2010. Petrogenesis and tectonic significance of the ~850 Ma Gangbian alkaline complex in South China: evidence from in situ zircon U–Pb dating, Hf–O isotopes and whole-rock geochemistry. Precambrian Research 114., 1–15.
Li, Z.X., Zhang, L.H., Powell, C.M.A., 1995. South China in Rodinia: part of the missing link between Australia-East Antarctica and Laurentia? Geology 23 (5), 407–410.
Li, Z.X., Li, X.H., Kinny, P.D., Wang, J., 1999. The breakup of Rodinia: did it start with a mantle plume beneath South China? Earth and Planetary Science Letters 173, 171–181.
Li, Z.X., Li, X.H., Zhou, H., Kinny, P.D., 2002. Grenvillian continental collision in South China: new SHRIMP U–Pb zircon results and implications for the configuration of Rodinia. Geology 30, 163–166.
Li, Z.X., Bogdanova, S.V., Collins, A.S., Davidson, A., DeWaele, B., Ernst, R.E., Fitzsimons, I.C.W., Fuck, R.A., Gladkochub, D.P., Jacobs, J., Karlstrom, K.E., Lu, S., Natapov, L.M., Pease, V., Pisarevsky, S.A., Thrane, K., Vernikovsky, V., 2008b. Assembly, configuration, and breakup history of Rodinia: a synthesis. Precambrian Research 160, 179–210.
Liang, X.R., Wei, G.J., Li, X.H., Liu, Y., 2003. Precise measurement of 143Nd/144Nd and Sm/Nd ratios using multiple-collectors inductively coupled plasma-mass spectrometer (MC-ICPMS). Geochimica 32, 91–96 (in Chinese with English abstract).
Liu, B.G., 1997. Analysis on the evolutionary features and origin of Shi'ershan superunit granite in Western Zhejiang. Geology of Zhejiang 13, 39–46 (in Chinese with English Abstract).
Ludwig, R., 2001. Users Manual for Isoplot/Ex rev. 2.49: A Geochronological Toolkit for Microsoft Excal. Berkeley Geochronology Center, Special Publication, No. 1a, 55 pp.
Luhr, J.F., Haldar, D., 2006. Barren Island Volcano (NE Indian Ocean): Island-arc high-alumina basalts produced by troctolite contamination. Journal of Volcanology and Geothermal Research 149, 177–212.
Ma, L.F., Qiao, X.F., Min, L.R., Fan, B.X., Ding, X.Z., 2002. Geological Atlas of China. Geological Publication House, Beijing, p. 372.
Ma, T.Q., Chen, L.X., Bai, D.Y., Zhou, K.J., Li, G., Wang, X.H., 2009. Zircon SHRIMP dating and geochemical characteristics of Neoproterozoic granites of southeastern Hunan. Geology in China 36 (1), 65–73 (in Chinese with English Abstract).
Maitre, R.W.L., Bateman, P., Dudek, A., Keller, J., Lemeyre, J., Bas, M.J.L., Sabine, P.A., Schmid, R., Sorensen, H., Streckeisen, A., Wooley, A.R., Zanettin, B., 1989. A Classification of Igneous Rocks and Glossary of Terms. Blackwell, Oxford.
McCulloch, M.T., Gamble, J.A., 1991. Geochemical and geodynamical constrains on subduction zone magmatism. Earth and Planetary Science Letters 102, 358–374.
Meschede, M., 1986. A method of discriminating between different types of mid-ocean ridge basalts and continental tholeiites with the Nb–Zr–Y diagrams. Chemical Geology 56, 207–218.
Pan, C.C., Feng, Y.H., Xu, G.W., 1988. On the Proterozoic Cangshuipu Group and the Cangshuipu orogeny in South China. Geology of Jiangxi 2 (2), 138–145 (in Chinese with English Abstract).
Pan, C.C., 2001. The evolution of the Cangshuipu Group and its lithostratigraphic problems on the bed successions of the Proterozoic Cangshuipu Group, Hunan Province, China. Geotectonica et Metallogenia 25 (2), 217–224 (in Chinese with English Abstract).
Pearce, J.A., 1975. Basalt geochemistry used to investigate past tectonic environments on Cyprus. Tectonophysics 25, 41–67.
Pearce, J.A., 1982. Trace element characteristics of lavas from destructive plate boundaries. In: Thorpe, R.S. (Ed.), Andesites. Wiley, Chicheater, pp. 525–548.
Pearce, J.A., Ernewein, M., Bloomer, S.H., Parson, L.M., Murton, B.J., Johnson, L.E., 1995. Geochemistry of the Lau Basin volcanic rocks: influence of ridge segmentation and arc proximity. In: Smellie, J.L. (Ed.), Volcanism Associated with Extension at Consuming Plate Margins. Special Contributions, vol. 81. Geological Society, London, pp. 53–75.
Pearce, J.M., Peate, D.W., 1995. Tectonic implications of the composition of volcanic arc magmatism. Annual Review of Earth and Planetary Sciences 23, 251–285.
Petrone, C.M., Ferrari, L., 2008. Quaternary adakite-Nb-enriched basalt association in the western Trans-Mexican Volcanic Belt: is there any slab melt evidence? Contributions to Mineralogy and Petrology 156, 73–86.
Pouclet, A., Lee, J.-S., Vidal, P., Cousens, B., Bellon, H., 1995. Cretaceous to Cenozoic volcanism in South Korea and in the Sea of Japan: magmatic constraints on the opening of the back-arc basin. In: Smellie, J.L. (Ed.), Volcanism Associated with Extension at Consuming Plate Margins. Geological Society of Special Publication, London, pp. 169–191.
Rolland, Y., Galoyan, G., Bosch, D., Sosson, M., Corsini, M., Fornari, M., Verati, C., 2009. Jurassic back-arc and Cretaceous hot-spot series In the Armenian ophiolites: implications for the obduction process. Lithos 112, 163–187.
Sandeman, H.A., Hanmer, S., Tella, S., Armitage, A.A., Davis, W.J., Ryand, J.J., 2006. Petrogenesis of Neoarchaean volcanic rocks of the MacQuoid supracrustal belt: a back-arc setting for the northwestern Hearne subdomain, western Churchill Province, Canada. Precambrian Research 144 (1–2), 126–139.
Seghedi, I., Downes, H., Szakács, A., Mason, P.R.D., Thirlwall, M.F., Rosu, E., Pécskay, Z., Márton, E., Panaiotu, C., 2004. Neogene–Quaternary magmatism and geodynamics in the Carpathian–Pannonian region: a synthesis. Lithos 72, 117–146.
Shinjo, R., Chung, S.L., Kato, Y., Kimura, M., 1999. Geochemical and Sr–Nd isotopic characteristics of volcanic rocks from the Okinwa Trough and Ryukyu Arc: implications for the evolution of a young, intracontinental back arc basin. Journal Geophysical Research 104 (B5), 10591–10608.
Shu, L.S., Zhou, G.Q., Shi, Y.S., Ying, Y., 1993. A study on the high pressure blueschist of eastern segment of Jiangnan erogenic belt and its geological age. Chinese Science Bulletin 38 (20), 1879–1882 (in Chinese with English Abstract).
Shu, L.S., Faure, M., Jiang, S.Y., Yang, Q., Wang, Y.J., 2006. SHRIMP zircon U–Pb age, litho- and biostratigraphic analyses of the Huaiyu Domain in South China—evidence for a Neoproterozoic orogen, not Late Paleozoic–Early Mesozoic collision. Episodes 29, 244–252.

Shu, L.S., Faure, M., Yu, J.H., Jahn, B.M., 2011. Geochronological and geochemical features of the Cathaysia block (South China): new evidence for the Neoproterozoic breakup of Rodinia. Precambrian Research 187, 263–276.
Shuto, K., Ishimoto, H., Hirahara, Y., Sato, M., Matsui, K., Fujibayashi, N., Takazawa, E., Yabuki, K., Sekine, M., Kato, M., Rezanov, A.I., 2006. Geochemical secular variation of magma source during Early to Middle Miocene time in the Niigata area, NE Japan: asthenosphere mantle upwelling during back-arc basin opening. Lithos 86, 1–33.
Song, B., Zhang, Y.H., Wan, Y.S., Jian, P., 2002. Mount making and procedure of the SHRIMP dating. Geology Review 48, 26–30 (Supplement in Chinese with English Abstract).
Sun, S.S., McDonough, W.F., 1989. Chemical and isotopic systematics of oceanic basalts: implication for mantle composition and process. In: Sauders, A.D., Norry, M.J. (Eds.), Magmatism in the Ocean Basins. Geological Society, London, pp. 313–345, Special Publications 42.
Tang, X.S., Huang, J.Z., Guo, L.Q., 1997. Hunan Banxi Group and its tectonic environment. Hunan Geology 16, 219–226 (in Chinese with English Abstract).
Taylor, B., Martinez, F., 2003. Back-arc basin basalt systematics. Earth and Planetary Science Letters 210, 481–497.
Teklay, M., 2006. Neoproterozoic arc–back-arc system analog to modern arc–back-arc systems: evidence from tholeiite–boninite association, serpentinite mudflows and across-arc geochemical trends in Eritrea, southern Arabian–Nubian shield. Precambrian Research 145 (5), 81–92.
Tian, L.Y., Castillo, P.R., Hawkins, J.W., Hilton, D.R., Hanan, B.B., Pietruszka, A.J., 2008. Major and trace element and Sr–Nd isotope signatures of lavas from the Central Lau Basin: implications for the nature and influence of subduction components in the back-arc mantle. Journal of Volcanology and Geothermal Research 178, 657–670.
Wang, J., Li, Z.X., 2003. History of Neoproterozoic rift basins in South China: implications for Rodinia breakup. Precambrian Research 122, 141–158.
Wang, J., Li, X.H., Duan, T.Z., Liu, D.Y., Song, B., Li, Z.W., Gao, Y.H., 2003a. Zircon SHRIMP U–Pb dating for the Cangshuipu volcanic rocks and its implications for the lower boundary age of the Nanhua strata in South China. Chinese Science Bulletin 48, 1663–1669.
Wang, L.J., Griffin, W.L., Yu, J.H., O'Reilly, S.Y., 2012a. Early crustal evolution in the western Yangtze Block: Evidence from U–Pb and Lu–Hf isotopes on detrital zircons from sedimentary rocks. Precambrian Research 222–223, 368–385.
Wang, X.C., Li, X.H., Li, Z.X., Li, Q.L., Tang, G.Q., Gao, Y.Y., Zhang, Q.R., Liu, Y., 2012b. Episodic Precambrian crust growth: Evidence from U–Pb ages and Hf-O isotopes of zircon in the Nanhua Basin, central South China. Precambrian Research 222–223, 386–403.
Wang, X.L., Zhou, J.C., Qiu, J.S., Gao, J.F., 2004. Geochemistry of the Meso- to Neoproterozoic basic-acid rocks from Hunan Province, South China: implications for the evolution of the western Jiangnan orogen. Precambrian Research 135, 79–103.
Wang, X.L., Zhou, J.C., Qiu, J.S., Zhang, W.L., Liu, X.M., Zhang, G.L., 2006. LA-ICP-MS U–Pb zircon geochronology of the Neoproterozoic igneous rocks from Northern Guangxi, South China: implications for petrogenesis and tectonic evolution. Precambrian Research 145 (1–2), 111–130.
Wang, X.L., Zhou, J.C., Griffin, W.L., Wang, R.C., Qiu, J.S., O'Reilly, S.Y., Xu, X.S., Liu, X.M., Zhang, G.L., 2007. Detrital zircon geochronology of Precambrian basement sequences in the Jiangnan orogen: dating the assembly of the Yangtze and Cathaysia blocks. Precambrian Research 159 (1–2), 117–131.
Wang, X.L., Zhou, J.C., Qiu, J.S., Jiang, S.Y., Shi, Y.R., 2008a. Geochronology and geochemistry of Neoproterozoic mafic rocks from western Hunan, South China: implications for petrogenesis and post-orogenic extension. Geology Magazine 145 (2), 215–233.
Wang, X.L., Zhao, G.C., Zhou, J.C., Liu, Y.S., Hu, J., 2008b. Geochronology and Hf isotopes of zircon from volcanic rocks of the Shuangqiaoshan Group, South China: implications for the Neoproterozoic tectonic evolution of the eastern Jiangnan orogen. Gondwana Research 14 (3), 355–367.
Wang, X.L., Jiang, S.Y., Dai, B.Z., Griffin, W.L., Dai, M.N., Yang, Y.H., 2011a. Age, geochemistry and tectonic setting of the Neoproterozoic (ca 830 Ma) gabbros on the southern margin of the North China Craton. Precambrian Research 190, 35–47.
Wang, X.L., Shu, L.S., Xing, G.F., Zhou, J.C., Tang, M., Shu, X.J., Qi, L., Hu, Y.H., 2012c. Post-orogenic extension in the eastern part of the Jiangnan orogen: evidence from ca 800–760 Ma volcanic rocks. Precambrian Research 222–223, 404–423.
Wang, W., Zhou, M.F., Yan, D.P., Li, J.W., 2012d. Depositional age, provenance, and tectonic setting of the Neoproterozoic Sibao Group, southeastern Yangtze Block, South China. Precambrian Research 192–195, 107–124.
Wang, Y.J., Fan, W.M., Guo, F., Peng, T.P., Li, C.W., 2003b. Geochemistry of Mesozoic mafic rocks around the Chenzhou–Linwu fault in South China: implication for the lithospheric boundary between the Yangtze and the Cathaysia Blocks. International Geology Review 45 (3), 263–286.
Wang, Y.J., Zhang, F.F., Fan, W.M., Zhang, G.W., Chen, S.Y., Cawood, P.A., Zhang, A.M., 2010. Tectonic setting of the South China Block in the early Paleozoic: resolving intracontinental and ocean closure models from detrital zircon U–Pb geochronology. Tectonics 29, http://dx.doi.org/10.1029/2010TC002750.
Wang, Y.J., Zhang, A.M., Fan, W.M., Zhao, G.C., Zhang, G.W., Zhang, F.F., Zhang, Y.Z., Li, S.Z., 2011b. Kwangsian crustal anatexis within the eastern South China Block: geochemical, zircon U–Pb geochronological and Hf isotopic fingerprints from the gneissoid granites of Wugong and Wuyi–Yunkai Domains. Lithos 127, 239–260.
Wang, Y.J., Zhang, A.M., Cawood, P.A., Fan, W.M., Xu, J.F., Zhang, G.W., Zhang, Y.Z. Geochronological, Geochemical and Nd-Hf-Os isotopic fingerprinting of an early Neoproterozoic arc-back-arc system in South China and its accretionary assembly along the margin of Rodinia. Precambrian Research, in press, http://dx.doi.org/10.1016/j.precamres.2013.03.020
Wang, Y.J., Zhang, A.M., Fan, W.M., Zhang, Y.H., Zhang, Y.Z., 2013. Origin of paleosubduction-modified mantle for Silurian gabbro in the Cathaysia Block: geochronological and geochemical evidence. Lithos 160–161, 37–54.
Wei, G.J., Liang, X.R., Li, X.H., Liu, Y., 2002. Precise measurement of Sr isotopic compositions of liquid and solid base using (LP) MC-ICP-MS. Geochimica 31 (3), 295–305.
Winchester, J.A., Floyd, P.A., 1977. Geochemical discrimination of different magma series and their differentiation products. Chemical Geology 20, 325–343.
Wood, D.A., Joron, J.L., Treuil, M., 1979. A re-appraisal of the use of trace elements to classify and discriminate between magma series erupted in different tectonic settings. Earth and Planetary Science Letters 45, 326–336.
Wood, D.A., 1980. The application of a Th–Hf–Ta diagram to problems of tectonomagmatic classification and to establishing the nature of crustal contamination of basaltic lavas of the British Tertiary volcanic province. Earth and Planetary Science Letters 50, 11–30.
Wu, R.X., Zheng, Y.F., Wu, Y.B., Zhao, Z.F., Zhang, S.B., Liu, X.M., Wu, F.Y., 2006. Reworking of juvenile crust: element and isotope evidence from Neoproterozoic granodiorite in South China. Precambrian Research 146, 179–212.
Wu, Y.B., Zheng, Y.F., Tang, J., Gong, B., Zhao, Z.F., Liu, X.M., 2007. Zircon U–Pb dating of water–rock interaction during Neoproterozoic rift magmatism in South China. Chemical Geology 246, 65–86.
Xia, X.P., Sun, M., Geng, H.Y., Sun, Y.L., Wang, Y.J., Zhao, G.C., 2011. Quasi-simultaneous determination of U–Pb and Hf isotope compositions of zircon by excimer laser-ablation multiple-collector ICPMS. Journal of Analytical Atomic Spectrometry 26, 1868–1871.
Xia, Y., Xu, X.S., Zhu, K.Y., 2012. Paleoproterozoic S- and A-type granites in southwestern Zhejiang: Magmatism, metamorphism and implications for the crustal evolution of the Cathaysia basement. Precambrian Research 216–219, 177–207.
Xu, B., Guo, L., Shi, Y., 1992. Proterozoic Terranes and Multiphase Collision Orogens in Anhui-Zhejiang-Jiangxi Ares. Geological Publishing House, Beijing, 112 pp.
Xu, X.S., Zhou, X.M., 1992. Precambrian S-type granitoids in South China and their geological significance. Journal of Nanjing University 28, 423–430 (in Chinese with English Abstract.).
Ye, M.F., Li, X.H., Li, W.X., Liu, Y., Li, Z.X., 2007. SHRIMP zircon U–Pb geochronologicaland whole-rock geochemical evidence for an early Neoproterozoic Sibaoan magmatic arc along the southeastern margin of the Yangtze Block. Gondwana Research 12, 144–156.
Yin, C.Y., Liu, D.Y., Gao, L.Z., Wang, Z.Q., Xing, Y.S., Jian, P., Shi, Y.R., 2003. Lower boundary age of the Nanhua System and the Gucheng glacial stage: evidence from SHRIMP II dating. Chinese Science Bulletin 16, 1657–1662.
Yu, J.H., O'Reilly, S.Y., Zhou, M.F., Griffin, W.L., Wang, L.J., 2012. U–Pb geochronology and Hf–Nd isotopic geochemistry of the Badu Complex, Southeastern China: Implications for the Precambrian crustal evolution and paleogeography of the Cathaysia Block. Precambrian Research 222–223, 424–449.
Zhang, C.H., Fan, W.M., Wang, Y.J., Peng, T.P., 2009. Geochronology and geochemistry of the Neoproterozoic mafic-ultramafic dykes in the Aikou area, western Hunan Province: Petrogenesis and its tectonic implications. Geotectonica et Metallogenia 33 (2), 283–293 (in Chinese with English Abstract).
Zhang, F.F., Wang, Y.J., Fan, W.M., Zhang, A.M., Zhang, Y.Z., 2011a. Zircon U–Pb geochronology and Hf isotopes of the Neoproterozoic granites in the central of Jiangnan Uplift. Geotectonica et Metallogenia 35 (1), 73–84 (in Chinese with English Abstract).
Zhang, Q.R., Li, X.H., Feng, L.J., Huang, J., Song, B., 2008. A new age constraint on the onset of the Neoproterozoic glaciations in the Yangtze platform, South China. The Journal of Geology 116, 423–429.
Zhang, S.B., Wu, R.X., Zheng, Y.F., 2012a. Neoproterozoic continental accretion in South China: Geochemical evidence from the Fuchuan ophiolite in the Jiangnan orogen. Precambrian Research 220–221, 45–64.
Zhang, Y.Z., Wang, Y.J., Fan, W.M., Zhang, A.M., Ma, L.Y., 2012b. Geochronological and geochemical constraints on the metasomatised source for the Neoproterozoic (~825 Ma) high-mg volcanic rocks from the Cangshuipu area (Hunan Province) along the Jiangnan domain and their tectonic implications. Precambrian Research 220–221, 139–157.
Zhang, Y.Z., Wang, Y.J., Fan, W.M., Zhang, A.M., Zhang, F.F., 2011b. Geochronological constraints on the Neoproterozoic collision along the Jiangnan uplift: evidence from studies on the Neoproterozoic basal conglomerates at the Cangshuipu area. Hunan Province. Geotectonica et Metallogenia 35 (1), 32–46 (in Chinese with English Abstract).
Zhao, G.C., Cawood, P.A., 1999. Tectonothermal evolution of the Mayuan assemblage in the Cathaysia Block: new evidence for Neoproterozoic collision-related assembly of the South China craton. American Journal of Science 299, 309–339.
Zhao, G.C., Cawood, P.A., 2012. Precambrian Geology of China. Precambrian Research 222–223, 13–54.
Zhao, G.C., Guo, J.H., 2012. Precambrian Geology of China: Preface. Precambrian Research 222–223, 1–12.
Zhao, J.H., Zhou, M.F., Yan, D.P., Zheng, J.P., Li, J.W., 2011. Reappraisal of the ages of Neoproterozoic strata in South China: no connection with the Grenvillian orogeny. Geology 39, 299–302.
Zheng, Y.F., Zhao, Z.F., Wu, Y.B., Zhang, S.B., Liu, X.M., Wu, F.Y., 2006. Zircon U–Pb age, Hf and O isotope constraints on protolith origin of ultrahigh-pressure eclogite and gneiss in the Dabie orogen. Chemical Geology 231, 135–138.

Zheng, Y.F., Zhang, S.B., Zhao, Z.F., Wu, Y.B., Li, X.H., Li, Z.X., Wu, F.Y., 2007. Contrasting zircon Hf and O isotopes in the two episodes of Neoproterozoic granitoids in South China: implications for growth and reworking of continental crust. Lithos 96, 127–150.
Zheng, Y.F., Wu, R.X., Wu, Y.B., Zhang, S.B., Yuan, H.L., Wu, F.Y., 2008. Rift melting of juvenile arc-derived crust: geochemical evidence from Neoproterozoic volcanic and granitic rocks in the Jiangnan Orogen, South China. Precambrian Research 163, 351–383.
Zheng, Y.F., 2012. Metamorphic chemical geodynamics in continental subdution zones. Chemical Geology 328, 5–48.
Zheng, Y.F., Xiao, W.J., Zhao, G.C., 2013. Introduction to tectonics in China. Gondwana Research 23, 1189–1206.
Zhong, Y.F., Ma, C.Q., She, Z.B., Lin, G.C., Xu, H.J., Wang, R.J., Yang, K.G., Liu, Q., 2005. SHRIMP U–Pb zircon geochronology of the Jiuling granitic complex batholith in Jiangxi Province. Earth Science 30 (6), 685–691 (in Chinese with English Abstract).
Zhou, J.C., Wang, X.L., Qiu, J.S., Gao, J.F., 2003. The discovery of Nanqiao highly depleted N-MORB and geological significance. Acta Petrologica et Mineralogica 22 (3), 211–216 (in Chinese with English Abstract).
Zhou, J.C., Wang, X.L., Qiu, J.S., Gao, J.F., 2004. Geochemistry of Meso- and Neoproterozoic mafic-ultramafic rocks from northern Guangxi, China: arc or plume magmatism? Geochemical Journal 38, 139–152.
Zhou, J.C., Wang, X.L., Qiu, J.S., 2009. Geochronology of Neoproterozoic mafic rocks and sandstones from northeastern Guizhou, South China: Coeval arc magmatism and sedimentation. Precambrian Research 170, 27–42.
Zimmer, M., Kroner, A., Jochum, K.P., Reischmann, T., Todt, W., 1995. The Gabal Gerf complex: a Precambrian N-MORB ophiolite in the Nubian Shield, NE Africa. Chemical Geology 123, 29–51.